DETERMINATION OF THE FOCAL LENGTH OF A LENS GENERATING ABERRATIONS

Ouma Emily Awuor

A Thesis Submitted to the Graduate School in Partial Fulfilment for the Requirements of the Degree of Master of Science in Physics of Egerton University

EGERTON UNIVERSITY

JANUARY, 2013.

DECLARATION AND RECOMMENDATION

DECLARATION

This thesis is my original work and has not been submitted for examinations in any other University.

Ouma Emily Awuor

Reg No. SM13/2443/09

Signature:_____ Date: _____

RECOMMENDATION

This thesis has been submitted to Graduate School with our approval as University supervisors.

Dr. Ndiritu. F. Gichuki

Egerton University.

Signature:_____ Date: _____

Dr. George Amolo

Chepkoilel University College.

Signature:_____ Date:_____

COPYRIGHT

ACKNOWLEDGEMENT

First of all my thanks, are directed to the Almighty God, for giving me grace and strength that enabled me to conclude this study. I sincerely acknowledge with gratitude all the people's assistance that made my study a success. My special thanks goes to my supervisors Dr. Ndiritu. F. Gichuki and Dr. George Amolo whose guidance, constructive suggestions, careful reading of my drafts, devotion, patience and encouragement contributed to my completing this Thesis. I also wish to thank Dr. Makau and Mr. Rop for the constructive corrections that they have given on my work. Of special mention is Prof. Forbes and Mr. Cosmas from the "Council of Scientific and Industrial Research (South Africa)" who provided me the facilities needed to do the experimental work of my project, patiently instructed me on the use of several equipment and together they supervised and corrected my laboratory work. My heartfelt gratitude goes to the entire staff of the Department of Physics, both at Egerton University and Chepkoilel University College for enabling me to overcome many unexpected hurdles during my study.

My family deserves special appreciation for their financial and emotional support and for being very understanding during the course of my work. Their encouragement and mostly prayers went a long way in giving me the courage to go on even when the going became very tough. I acknowledge the total and unreserved assistance accorded to me by classmates without whose selfless and sacrificial support I would never have gotten this far.

Finally, the financial assistance rendered by The National Laser Centre, South Africa during the duration of performing my experiments in their laboratories is gratefully acknowledged.

ABSTRACT

In most laser applications it is necessary to focus, modify or shape the laser beam by using lenses and other optical elements. The most important characteristic of a lens is its focal length. The focal length of a lens gives a measure of how strongly the lens either converges or diverges light. When the lens is imperfect, it generates aberrations. This imperfection could be due to disfigured or imperfectly figured optics and misalignments of the lens in an optical system. It's important to determine how the aberrations affect the focal length and hence the imaging properties of the lens and find ways of minimizing or eliminating these effects. This will improve the quality of the experiments and results achieved. Also in case of imperfect lenses e.g. those with cracked or deformed surfaces, cost of new purchases will be saved in that the imperfect lenses can still be used and the aberrations generated corrected. This thesis reports a theoretical and experimental investigation of the focal length of a lens generating aberrations. A theoretical model was formulated by considering the general case of a Gaussian laser beam passing through a lens with arbitrary aberrations and finite aperture. By considering the difference between the incoming and outgoing effective radii of curvature, an expression for the lens focal length as a function of the aberrations present was derived. In order to test the model, a lens with various aberrations was simulated with phase holograms in the laboratory. Primary aberrations with selected coefficients were programmed onto a phase Spatial Light Modulator whose Liquid Crystal Display (LCD) was active in reflective mode only. On striking the LCD, the incoming laser beam was reflected off it and into a two-dimensional Shack-Hartmann wavefront sensor. The sensor used binary optic lenslet arrays to directly measure the wavefront slope (phase gradient) of the laser beam. By integrating these measurements over the lens aperture, the wavefront or phase distribution was determined and the laser beam parameters presented in terms of Zernike polynomial coefficients. From these, Zernike primary aberrations affecting the field curvature immediately before and after the lens which in turn affects the accurate determination of its focal length was analysed from the graphs of lens power against aberrations and calculated using Mathematica software. The theoretical results show that out of all the primary aberrations used, only three, namely spherical, defocus and x-astigmatism aberrations have significant effect on the lens focal length. The presence of x- astigmatism creates two focal planes, one in the horizontal plane and the other in the vertical plane. This means that if x-astigmatism is non zero then the lens will have two focal planes. The experimental result validates the theoretical model satisfactorily.

TABLE OF CONTENTS

LIST OF TABLES

LIST OF FIGURES

LIST OF ACCRONYMS

ϕ - Wavefront phase

a – Aperture radius

A_{nm} – Coefficient of aberrations

f - Focal length

m – Frequency of wavefront

n - Function of wavefront along meridians

R_f – Curvature of field behind the lens

R_i – Curvature of field in front of lens

γ - Truncation parameter

θ - Angular coordinate of the wavefront

λ - Wavelength

ρ – Radial coordinate of the wavefront

CHAPTER ONE

1.0 INTRODUCTION

1.1 Background Information

In the study of transmission and reflection of light through an optical system it is often advantageous to consider the paraxial approximation in which the beam travels along an optical axis and directions close to it. In such a context the illumination may be identified as a combination of axial waves of light for which the angles are all small. If a typical angle is θ radians, it designates the situation in which cosine θ may be well approximated by $1-\frac{1}{2}\theta^2$ as paraxial (Sudarshan *et.al*, 1983). A common situation in which the paraxial approach fails is when aberrations are present. Aberrations are departures of the performance of an optical system from the predictions of paraxial optics. They occur when light from one point of an object after transmission through the system does not converge into (or does not diverge from) a single point. This leads to blurring of the image produced by an image-forming optical system. There are several causes of aberration such as,

i. Disfigured or imperfectly figured optics since rarely is an element made exactly to specifications.
ii. Misalignments. If the mirrors in a multiple-element system are not perfectly aligned, aberrations will result. These can be derived (third-order) from the aberration expressions for decentred elements.
iii. Forced surface deformations caused by thermal variations and improper mounting.
iv. Air currents / turbulence.

For a laser beam propagating in the Gaussian form, i.e. a beam whose intensity is highest at the centre and diminishes around the edges, it is more appropriate to introduce the aberrations as a phase function that modifies the wavefront of a laser beam. A wavefront is the surface that is normal to the direction of propagation of light, and it represents all the points of an oscillating electric field having equal phase. Since the phase function is usually located at the exit pupil of the optical system then it means that the departure of the actual wavefront is with respect to an ideal spherical wavefront given by paraxial optics, (Alda *et.al*, 1997).

A lens is the most basic optical imaging device available to an optics researcher. The focal length is the most important parameter in the optical performance of a lens. Several methods

are available for the measurement of the focal length which includes determining the change of curvature of the field immediately before and after the lens. If aberrations are present in the lens then the curvature is defined as the average curvature of the field. The optical lens has been studied previously in terms of classical optics to determine its aberrations (Mahajan, 1998). Yet to date no study has been done to link the aberrations of the lens to its focal length. This work attempts to formulate a simple formula that can be used to determine the focal length of an aberrated lens based on the analysis of the input and output laser beams. A general case of a Gaussian laser beam passing through a lens with arbitrary aberrations and finite aperture will be considered. By noting the difference in the incoming and outgoing effective radius of curvatures, an expression for the focal length as a function of the aberrations in the beam will be derived.

To achieve this experimentally, a two dimensional Shack-Hartmann wavefront sensor that uses Zernike polynomials to expand the wavefront aberrations was used. The primary or low order Zernike polynomials are related to these aberrations up to a third order: tilt, astigmatism, spherical, triangular astigmatism, defocus and coma aberrations. The wavefront sensor gives its measurements in terms of Cartesian coordinates i.e. the x and y axis although the laser beam has a cylindrical geometry. The measurements provide the required data for evaluation of the influence of aberrations in the lens focal length. This influence can be deduced from the formalism presented in this thesis.

This work is organised as follows. Chapter one gives the introduction. Chapter two details the historical background of the work, followed by the theory of aberrations and the theoretical model for calculating the focal length including the tensor formulation used to calculate beam size and curvature in both cartesian and cylindrical form. In chapter three, the experimental methods together with the equipment used are presented. Chapter four gives the results, analysis and discussion. Finally conclusion, recommendations and references are presented.

1.2 Statement of the Problem

In optical experiments using lenses, it's important to know how the lens focal length impacts on the laser beam that is transmitted through it. In some cases the lens is imperfect and therefore generates aberrations which have effects on individual or collective property of the laser beam. Hence there is need to determine which specific aberrations being generated have an effect on the lens focal length and how to correct for the aberrations so as to improve the quality of the image formed.

1.3 Objectives

1.3.1 General Objective

To determine how the aberrations generated by an imperfect lens in any optical system affects the focal length of the lens together with the imaging properties of the lens and how to minimise or eliminate these undesirable effects.

1.3.2 Specific Objectives

(i). Determine how the primary aberrations affect the curvature of the lens field immediately in front and after the lens.

(ii). Develop a theoretical model for calculating the focal length of a lens generating aberrations.

(iii). To test the formulated theoretical model.

1.4 Hypotheses

(i). None of the primary aberrations have an effect on the curvature of the field surrounding the lens.

(ii). Not all the primary aberrations used to formulate the theoretical model affect the lens focal length.

(iii). The theoretical and experimental results are a reasonable match.

1.5 Justification of the Study

There is continued need to know the properties of optical devices especially lenses in the expanding optical industry. The quality of image formed has been associated with the nature of the lenses used, some of which introduces aberrations. As such, it is important to understand these so that it will be easier to identify, correct or compensate for aberrations in any optical system. This will improve the quality of the experiments and results achieved. Also in case of imperfect lenses e.g. those with cracked or deformed surfaces, cost of new purchases will be saved in that the imperfect lenses can still be used and the aberrations generated corrected using the theoretical model developed.

CHAPTER TWO

2.0 LITERATURE REVIEW

The propagation of light through aberrated optical systems is a subject which has elicited much interest in the last few years. For most optical systems of practical interest a complete analytical treatment of the aberrations is not possible. The primary aberrations obtained by considering the aberration function to be expanded as a polynomial in the aperture can be calculated numerically. Optical aberrations have found use in the fields of atmospheric turbulence (Noll, 1976), imaging (Mahajan, 1998) and ophthalmology (Dai, 2008). Their use in laser beams has mostly been limited to the aberrations' impact on the laser field during propagation (Wada *et. al*., 2005 and Singh *et. al*., 2007).

A polynomial representation of the optical wavefront is essential in the analysis of optical system performance (Born and Wolf, 1999). Use of the well-known Zernike polynomials for describing aberrations of an optical system is acceptable since they are related to the primary aberrations and thus provide a convenient mathematical expression of the aberration content in a wavefront using familiar terms (Tripoli, 2002). As an example, Bezdid'ko (1974) reviewed the use of these polynomials in the analysis of wavefront aberrations. In particular he demonstrated that the coefficients of the Zernike polynomial expansion of the wavefront aberration tells us the degree to which higher order aberrations are compensated by the lower ones. Wang and Markey (1977) used these polynomials to represent the Kolmogoroff spectrum of atmospheric turbulence, from which the numbers of independent corrections required in a wavefront compensated system are derived. Noll (1976) also introduced several new parameters of these polynomials. Today these polynomials are in widespread use in optical design as well as in optical testing (Francis and Harvey, 1976).

For an optical system having a rotational symmetry the primary or Seidel aberrations are five in number. These are aberrations which are due to the geometry of lenses or mirrors, and are applicable to systems dealing with monochromatic light (James and Katherine, 1992). Equations that can be used to calculate Seidel aberrations generated by a lens, based on its focal length, geometry, object and image positions were derived by Mahajan (1991). The equations show that out of the five aberrations only four are generated that is, coma, field curvature, astigmatism and spherical aberration. This formulation in part was used by Ruff and Siegman (1993) to derive a simple formula showing the effects of spherical aberration on laser beam quality factor M^2 and that there was a critical size of the beam above which the

beam degraded quickly. This model was extended to a tensor formulation to include all primary Zernike coefficients in the characterization not only of beam quality but also of divergence and curvature but was not tested experimentally (Alda et al, 1997).

2.1 Wavefront Aberrations

The deviation of a wavefront in an optical system from a desired perfect planar wavefront is called wavefront aberration. The exit pupil plane is the plane that usually describes these aberrations (Robert *et al*, 2000). The phase of a wavefront can be expressed as $\phi(x,y) = \frac{2\pi}{\lambda} W(x,y)$ where the function *W(x,y)* measured in waves represents the optical path difference between the actual (aberrated wavefront) and a reference (non-aberrated) one. For an optical system that is rotationally symmetric about its optical axis, the number of aberration terms through a certain order *i* is given by (Jason, 2010),

$$N_i = \frac{(i+2)(i+4)}{8}. \qquad (1)$$

The number of aberration terms through the fourth order $i = 4$, is now equal to six. They consist of piston aberration and the terms that correspond to the five seidel aberrations.

2.2 Seidel Aberrations

The Seidel or primary aberration function ($n + m \leq 4$) corresponds to $i = 4$ and its reduced form is given by (Mahajan, 1998);

$$W(\rho,\theta) = a_{40}\rho^4 + a_{31}\rho^3 \cos\theta + a_{22}\rho^2 \cos^2\theta + a_{20}\rho^2 + a_{11}\rho\cos\theta, \qquad (2)$$

where a_{nm} are the peak aberration coefficients representing the maximum value of the corresponding aberration. The aberrations together with their descriptions are listed in Table 1. Note that the piston term with $n = m = 0$ does not constitute an aberration although it is counted as such in equation (1). The indices n and m simply describe the function of the wavefront along meridians and frequency of the aberration respectively, while ρ gives the radial coordinate and θ is the angular coordinate of the aberrations.

Table 1: Primary aberrations in a simplified form; $i = 4$, $n + m \leq 4$, (Mahajan, 1998).

n	**m**	**Aberration Term** $a_{nm}\rho^{n}Cos^{m}\theta$	**Aberration Name**
1	1	$a_{11}\rho Cos\theta$	Distortion
2	0	$a_{20}\rho^{2}$	Defocus
2	2	$a_{22}\rho^{2}Cos^{2}\theta$	Astigmatism
3	1	$a_{31}\rho^{3}Cos\theta$	Coma
4	0	$a_{40}\rho^{4}$	Spherical

2.3 Balanced Aberrations

In the absence of aberrations, the intensity is a maximum at the Gaussian image point. If aberrations are present, this will in general no longer be the case. The point of maximum intensity is called diffraction focus, and for small aberrations is obtained by finding the appropriate amount of tilt and defocus to be added to the wavefront so that the wavefront variance is a minimum. The ratio of intensity at the Gaussian image point in the presence of aberration, to the intensity that would be obtained if no aberrations were present, is called the Strehl ratio. Since the Strehl ratio is higher for smaller aberration variance, a given aberration is mixed with one or more lower-order aberrations to reduce its variance. This process is known as aberration balancing, (Mahajan, 1991). Consider, for example, balancing of spherical aberration with defocus:

$$\phi(\rho) = A_s\rho^{4} + B_d\rho^{2}, \tag{3}$$

where A_s and B_d denotes the value of peak aberrations for spherical and defocus aberrations respectively. Its variance is calculated as follows (Mahajan, 1998);

$$\sigma^{2}\phi = \left\langle \phi^{2} \right\rangle - \left\langle \phi \right\rangle^{2}$$

$$\left\langle \phi \right\rangle = \frac{1}{\pi}\int_{0}^{1}\int_{0}^{2\pi}\left(A_s\rho^{4} + B_d\rho^{2}\right)\rho d\rho d\theta$$

$$= 2\int_0^1 \left(A_s \rho^5 + B_d \rho^3\right) d\rho$$

$$= \frac{A_s}{3} + \frac{B_d}{2}.$$

$$\left\langle \phi^2 \right\rangle = \frac{1}{\pi}\int_0^1 \int_0^{2\pi} \left(A_s \rho^4 + B_d \rho^2\right)^2 \rho d\rho d\theta$$

$$= 2\int_0^1 \left(A_s^2 \rho^9 + B_d^2 \rho^5 + 2A_s B_d \rho^7\right) d\rho$$

$$= \frac{A_s^2}{5} + \frac{B_d^2}{3} + \frac{A_s B_d}{2}.$$

$$\sigma^2\phi = \frac{4A_s^2}{45} + \frac{B_d^2}{12} + \frac{A_s B_d}{6}. \qquad (4)$$

The value of B_d for minimum variance will be given by:

$$0 = \frac{\partial \sigma^2 \phi}{\partial B_d} = \frac{1}{6}\left(B_d + A_s\right).$$

This implies that $B_d = -A_s$. For balanced spherical aberration Eqn. (3) becomes,

$$\phi_{bs} = A_s\left(\rho^4 - \rho^2\right); \quad \sigma^2\phi_{bs} = \frac{A_s^2}{180} \qquad (5)$$

Without balancing with defocus;

$$\phi_s(\rho) = A_s \rho^4; \sigma^2\phi_s = \frac{4A_s^2}{45}. \qquad (6)$$

From Eqn. (5), the balancing of spherical aberration with defocus reduces its variance by a factor of 16, or the standard deviation by a factor of 4. Hence aberration tolerance for a given Strehl ratio increases by a factor 4. Similarly coma can be balanced with tilt, and astigmatism with defocus.

2.4 Balanced Aberrations and Zernike Circle Polynomials

In analysing the effect of aberrations on an imaging system, it is advantageous to represent the phase of the corrupted optical wave in a series of simple orthogonal functions. This approach was first used in the description of fixed aberrations where the phase was

expanded using the lower order polynomials (Wang and Markey, 1977). Zernike polynomials are mathematical expressions fitted to three dimensional data to describe the aberrations of wavefront measurements. A formula containing Zernike polynomials is fitted to a wavefront with unknown optical properties i.e. one emanating from an arbitrary lens. To fit the formula the coefficients of best fit are found for each polynomial. These coefficients can then be thought of as the amount of specific aberrations in the wavefront (Tripoli, 2002). The Zernike polynomials as introduced by Noll (1976), represent a set of functions of two variables that are orthogonal over a circle with unit radius a. It is customary to define these polynomials as a product of two functions, one depending on a radial coordinate ρ and the other depending only on the angular coordinate θ. Each Zernike term can be represented by,

$$Z_n^m(\rho,\theta) = C_n^m R_n^m(\rho)\Theta_m(\theta), \tag{7}$$

where both m and n are integers, $n \geq 0$, $-n \leq m \leq n$, $0 \leq \rho \leq 1$, $0 \leq \theta \leq 2\pi$ and $n \pm m$ is even. The radial polynomial is defined by, (Larry and Ronald, 2005):

$$R_m^n(\rho) = \sum_{k=0}^{\frac{n-m}{2}} \frac{(-1)^k (n-k)\rho^{n-2k}}{k!(\frac{n+m}{2}-k)!(\frac{n-m}{2}-k)!}. \tag{8}$$

The index n represents the radial degree or order of the polynomial since it represents the highest power of ρ in the polynomial and m is the azimuthal frequency. The polynomial is even if m is even and odd if m is odd. The orthogonality property of this polynomial is

$$\int_0^1 \int_0^{2\pi} Z_n^m(\rho,\theta) Z_k^{m*}(\rho,\theta)\rho d\theta d\rho = \frac{\pi}{n+1}\delta_{nk} = \begin{cases} \pi/(n+1), k=n \\ 0, k \neq n \end{cases}. \tag{9}$$

where * denotes complex conjugate and δ_{nk} is the kronecker delta. Virtually any realistic wavefront phase $\phi(\rho,\theta)$ can be represented in a 2 dimensional series of Zernike polynomials as;

$$\phi(\rho,\theta) = A_{00} + \sum_{n=2}^{\infty} A_{0n} R_n^0(\rho) + \sum_{n=0}^{\infty}\sum_{m=1}^{n} (A_{mn} Cosm\ \theta + B_{mn} Sinm\ \theta) R_n^m(\rho), \tag{10}$$

where A_{nm} and B_{nm} are individual polynomial coefficients referred to as the even and odd terms respectively. They are given by;

$$A_{nm} = \frac{1}{\pi}\sqrt{\frac{2(n+1)}{1+\delta_{m0}}}\int_0^{2\pi}\phi(\rho,\theta)R_{nm}Cos(m\theta)\rho d\rho d\theta$$

$$B_{nm} = \frac{1}{\pi}\sqrt{\frac{2(n+1)}{1+\delta_{m0}}}\int_0^{2\pi}\phi(\rho,\theta)R_{nm}Sin(m\theta)\rho d\rho d\theta.$$

Because of their orthogonality, the aberration terms of a Zernike polynomial expansion are referred to as the orthogonal aberrations. The aberration function may also be written in terms of orthonormal Zernike circle polynomials $Z_j(\rho,\theta)$ in the form (Mahajan, 1994),

$$\phi(\rho,\theta) = 2\pi\sum_{j=1}^{\infty} C_j Z_j(\rho,\theta), \qquad (11)$$

where the index *j* is a polynomial-ordering number, which is a function of both *n* and *m*, C_j is the expansion or aberration coefficient, and

$$Z_{evenj}(\rho,\theta) = \sqrt{2(n+1)}R_n^m(\rho)Cosm\theta \qquad m\neq 0, \qquad (12a)$$

$$Z_{oddj}(\rho,\theta) = \sqrt{2(n+1)}R_n^m(\rho)Sinm\theta \qquad m\neq 0, \qquad (12b)$$

$$Z_j(\rho,\theta) = \sqrt{n+1}R_n^0(\rho) \qquad m=0. \qquad (12c)$$

The orthonormality of Zernike polynomials implies that

$$\int_0^1\int_0^{2\pi} Z_j(\rho,\theta)Z_{j'}(\rho,\theta)\rho d\rho d\theta \;/\; \int_0^1\int_0^{2\pi}\rho d\rho d\theta = \delta_{jj'} \qquad (13)$$

The expansion coefficients C_j are given by

$$C_j = \pi^{-1}\int_0^1\int_0^{2\pi}\phi(\rho,\theta)Z_j(\rho,\theta)\rho d\rho d\theta. \qquad (14)$$

Table 2 shows the ordering of the third order aberrations and the relationships among the indices *j*, *n* and *m*. For a given value of *n*, a polynomial with a lower value of *m* is ordered first.

Each orthogonal aberration is made up of one or more classical aberrations of a higher degree which is optimally balanced with those of equal or lower degree such that its variance across the pupil is balanced. For this reason Zernike polynomial aberration may also be referred to as a balanced aberration.

Table 2: Aberrations corresponding to the orthonormal Zernike circle polynomials $Z_j(\rho,\theta)$ (Mahajan, 2007).

j	***n***	***m***	**Orthonormal Zernike Polynomial** $Z_j(\rho,\theta) \equiv Z_n^m(\rho,\theta) = \left[\frac{2(n+1)}{1+\delta_{m0}}\right]^{1/2} R_n^m(\rho)Cosm\theta$	**Zernike Aberration Name**
1	0	0	1	Piston
2	1	1	$2\rho\cos\theta$	Distortion (*x*-tilt)
3	1	1	$2\rho\sin\theta$	Distortion (*y*-tilt)
4	2	0	$\sqrt{3}(2\rho^2-1)$	Field curvature (defocus)
5	2	2	$\sqrt{6}\rho^2\sin 2\theta$	Primary astigmatism at 45^0
6	2	2	$\sqrt{6}\rho^2\cos 2\theta$	Primary astigmatism at 0^0
7	3	1	$\sqrt{8}(3\rho^3-2\rho)\sin\theta$	Primary *y* coma
8	3	1	$\sqrt{8}(3\rho^3-2\rho)\cos\theta$	Primary *x* coma
9	3	3	$\sqrt{8}\rho^3\sin 3\theta$	*y*-Triangular astigmatism
10	3	3	$\sqrt{8}\rho^3\cos 3\theta$	*x*-Triangular astigmatism
11	4	0	$\sqrt{5}(6\rho^4-6\rho^2+1)$	Primary spherical

For example, the Zernike primary spherical aberration $R_4^0(\rho)$ consists of a classical primary spherical aberration (ρ^4 term) optimally balanced with defocus (ρ^2 term) to minimize its variance. It may be called balanced primary spherical aberration. The Zernike primary coma $R_1^3(\rho)Cos\theta$ consists of classical primary coma ($\rho^3Cos\theta$ term) optimally balanced with tilt ($\rho Cos\theta$ term) and may be called balanced coma while the Zernike primary astigmatism $R_2^2(\rho)Cos2\theta$ consists of classical primary astigmatism ($\rho^2Cos^2\theta$ term) optimally balanced with defocus.

The Zernike polynomials are unique in that they are the only complete set of polynomials in two coordinate variables ρ and θ that are (a) orthogonal over a unit circle, (b) are invariant in form with respect to rotation of the axes about the origin, and (c) includes a polynomial for each permissible pair of *n* and *m* values (Mahajan, 2007).

2.5 Aberration Variance

A useful property of the Zernike series Eqn. (10) is that the root mean square (*rms*) wavefront error due to primary (low-order) aberrations can readily be calculated. If all the coefficients in Eqn.(10) are known, the geometric sum of the non-piston terms yields the wavefront variance or mean square deformation (Larry and Ronald, 2005),

$$(\Delta\phi)^2 = \frac{1}{\pi}\int_0^1\int_0^{2\pi} \rho\left[\phi(\rho,\theta) - \left\langle\phi(\rho,\theta)\right\rangle\right]^2 d\theta\, d\rho$$

$$= \sum_{n=1}^{\infty}\sum_{m=-n}^{n} \frac{\left|C_{mn}\right|^2}{n+1}. \qquad (15)$$

The square root of which gives the *rms* wavefront error.

2.6 Combination of Field Curvature and the Rest of Primary Aberrations

Field curvature (defocus) is inherent in every optical system and is related to the lens surface and its index of refraction. Field curvature is an image defect that causes off axis image wavefronts to focus in different focal planes other than the ideal image plane. Positive lens exhibit 'inward' field curvature i.e. the image formed has an out of focus condition at the edge of the field when the lens is sharply focused on the axis. Negative lenses have outward curving fields. This defect can be corrected to some extent by combining positive and negative lens elements. If no other aberrations are present the images formed are true point images on a curved image surface called the Petzval surface.

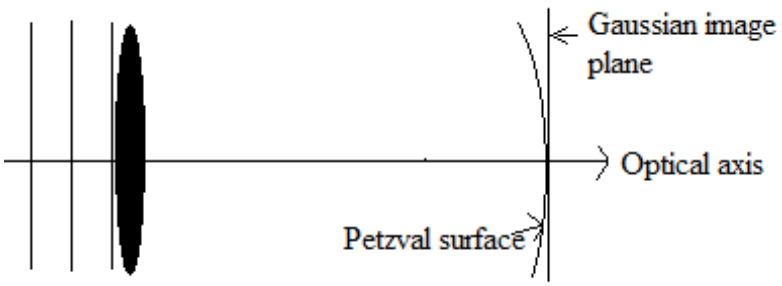

Figure. 1 Field curvature (defocus).

In the presence of astigmatism aberration, the elliptical distortion of the image point increases with increasing off-axial distance. Two separate astigmatic focal surfaces corresponding to both the tangential and sagittal conjugates will be formed. Both the tangential and sagittal image surfaces are on the same side of the Petzval surfaces with the tangential image surface three times as far from the Petzval surface as the sagittal image surface.

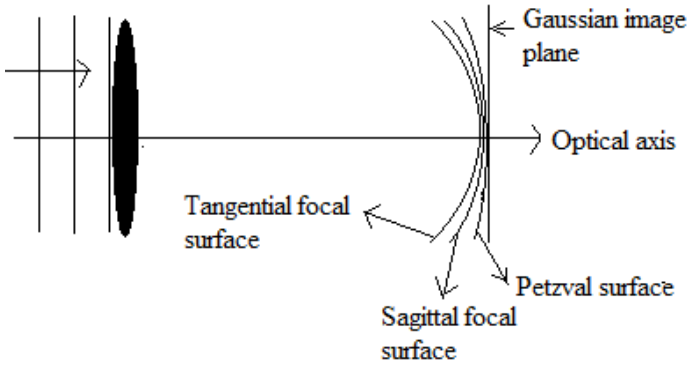

Figure.2 Imaging in presence of defocus and astigmatism, (James and Katherine, 1992).

Geometrical distortion is an aberration that does not affect image sharpness but instead the parts of an extended image are just in the wrong places. In a distorted image straight lines in an object are imaged as curved lines therefore distortion only applies when a lens is imaging a flat object surface onto a flat image surface. In the presence of field curvature the image surface formed is a curved plane, so distortion is not defined but a mapping function can instead be determined.

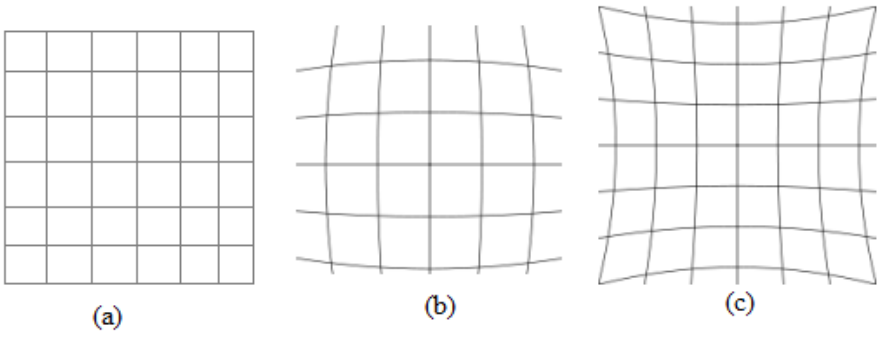

Figure.3 (a) Rectangular object while (b) and (c) are images with barrel and pincushion distortion, respectively.

Spherical aberration is a failure of focus caused when rays that are parallel to the optical axis have different focal lengths at different image field heights. This aberration usually has a uniform effect across the entire image area even in the presence of field curvature aberration.

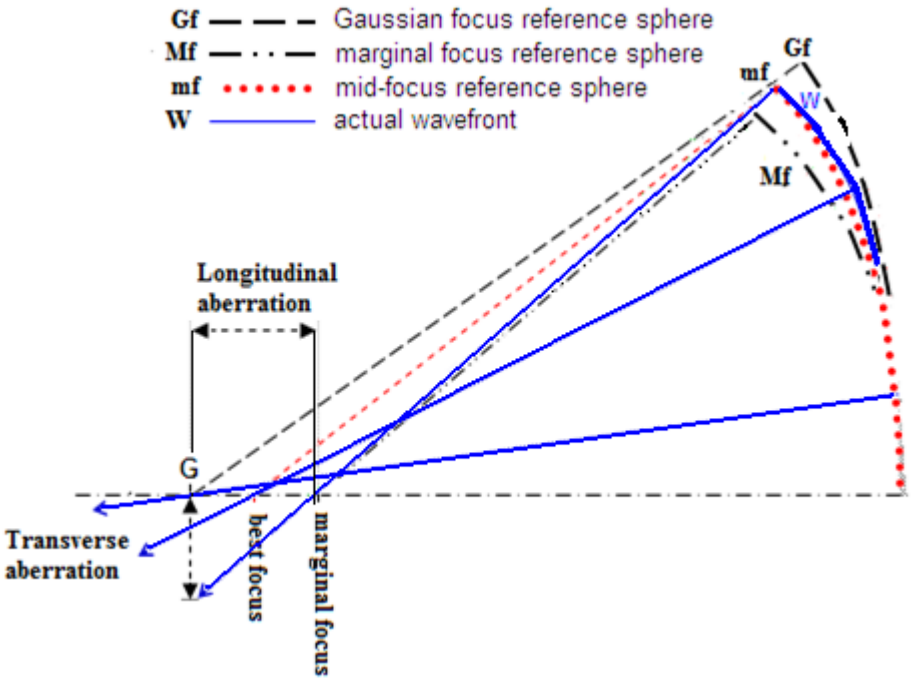

Figure4. Spherical aberration of a concave spherical lens, (Telescope-optics.net).

Coma is a failure to magnify equally the rays of light passing through opposite sides of the lens objective or eyepiece. Coma is absent on the optical axis and becomes more severe as image field height increases. It also produces elongated and expanded 'tails' that extend radially from point images or luminance edges in off-axis light and that increases in size with field height. In the presence of field curvature the image retains its 'comatic' shape, since the image plane is already curved and this matches the curved plane caused by the field curvature.

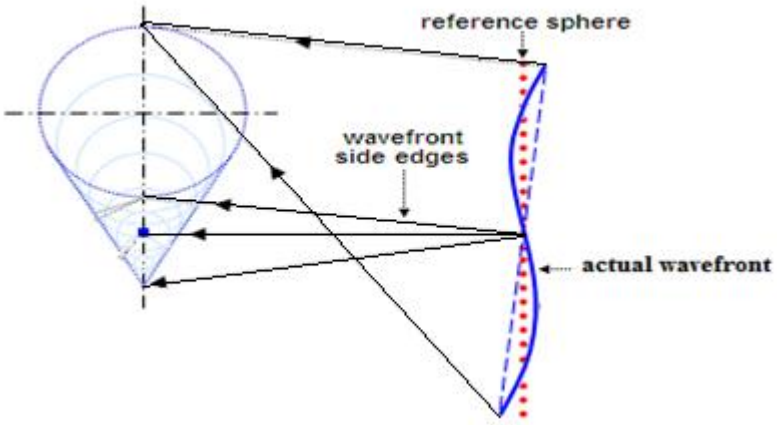

Figure 5. Illustration of the comatic wavefront deformation, and how it causes rays to spread into a comatic blur, (Telescope-optics.net).

CHAPTER THREE

3.0 MATERIALS AND METHODS

The experimental part of this work was done at the National Laser Centre Laboratories located in the Council for Scientific and Industrial Research (CSIR), Pretoria South Africa. This involved the use of a phase only Spatial Light Modulator (SLM) and a two dimensional wavefront sensor (Shack-Hartmann).

3.1 Spatial Light Modulator

The model used was PLUTO SLM shown in Figure 6. The SLM is a device that consists of a liquid crystal display (LCD) which is programmed and addressed by an electronic circuit. The LCD is the most essential part of the SLM and comprises of 1920 by 1080 pixels each having a dimension of 8µm. The mechanism of the display is based on electrically controlled birefringence (Karim, 1990). Each pixel is addressed by two electrodes and the molecules making up the pixels are aligned parallel to the electrodes. When an electric field is applied to the electrodes, the molecules are forced to tilt in the direction of the field. The size of the field is mostly in a range of zero to a given maximum. The incident light is polarized linearly parallel to the axis of the liquid crystal molecules. When the molecules tilt in the direction of the applied field, the refractive index seen by the light changes accordingly and consequently so does its phase (Konforti *et.al*, 1988). Zero electric field would correspond to no change in phase while a maximum electric field gives a 2π radian phase change.

Figure. 6 The PLUTO Spatial Light Modulator, (Holoeye photonics).

The phase screens of the primary Zernike aberrations described in Table 2 section 2.4, were obtained using a Mathematica code shown in Appendix A. These were then programmed on

the SLM and imprinted on the laser beam reflected off the LCD. The Zernike coefficients were then obtained by using a wavefront sensor.

3.2 Shack-Hartmann Two Dimensional Wavefront Sensor

At any point in time, the electric field of a coherent light travelling along the z-axis can be represented by $E(\rho,\theta) = \left(\frac{2\gamma^2}{\pi a^2}\right)^{\frac{1}{4}} \exp(-\gamma^2\rho^2)\exp(i\phi(\rho,\theta))$, where γ is the truncation parameter, *a* is the aperture radius and ϕ is the phase measured with reference to a point on the *z*-axis. Because of rapid oscillations at various optical frequencies it is not possible to directly measure the electric field. However, by using a Shack-Hartmann wavefront sensor, the electric field at a given plane normal to the z-axis is indirectly reconstructed and approximated by measuring both the phase and intensity of an incident light wave, (Neal *et al*, 2002). The basic geometry of a Shack-Hartmann wavefront sensor is illustrated in Figure 7 (a). The sensor consists of two basic parts: a lenslet array and a CCD detector. For an incoming incident light the lenslet array creates a number of separated focal spots on the detector which determines the exact position of the focal spots. The position of these focal spots is directly related to the average wavefront slope over each lenslet aperture. Thus the pattern of the spots at the focal plane gives information about the spatially resolved wavefront that can be integrated to reconstruct the wavefront (Neal et al, 1997).

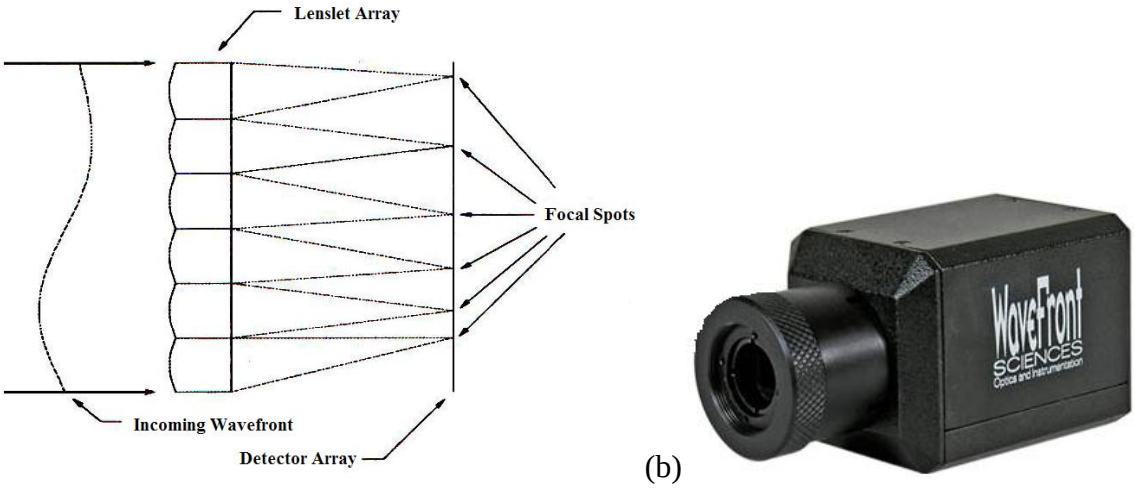

(a) (b)

Figure.7 (a) Basic configuration of a wavefront sensor and (b) Wavefront sciences CLASS 2D Shack-Hartmann wavefront sensor, (AMO wavefront sciences).

There are three basic steps to the analysis process; determination of the focal spots position, conversion to wavefront slopes and wavefront reconstruction (Neal *et al*, 1996).

(i) Spot Position

This is determined by using the centre of mass algorithm to measure photon concentration or light intensity, *I*, on the detector array. For a given irradiance distribution the spot positions x_i and y_i are found by,

$$x_i = \frac{\sum x_i I_i}{\sum I_i} \qquad \text{and} \quad y_i = \frac{\sum y_i I_i}{\sum I_i}. \tag{16}$$

(ii) Wavefront Slope

This is determined by comparison of the measured centroids to a reference wavefront. For a set of measured centroids (x_i,y_i) and reference centroids (x_j,y_j) the wavefront slope distribution is given by

$$\begin{pmatrix} \partial w / & dx \\ \partial w / & \partial y \end{pmatrix} = \frac{1}{f}\begin{pmatrix} x_i & -x_j \\ y_i & -y_j \end{pmatrix}, \text{ where } f \text{ is the lenslet focal length.} \tag{17}$$

(iii) Wavefront Reconstruction

The wavefront is related to the slope through the definition of the gradient, i.e.

$$\nabla w = \frac{\partial w}{\partial x}\hat{i} + \frac{\partial w}{\partial y}\hat{j}. \tag{18}$$

The derivatives are approximated by the average over the lenslet area. One method of reconstructing the wavefront from the slope measurement is the modal (polynomial fitting) method. Here, the method is described in terms of functions that have analytic derivatives. The measured slope data is then fitted to the derivatives of these functions, allowing a direct determination of the wavefront from the fitted coefficients. For example if the wavefront at a point (x,y) is written in terms of the Zernike polynomial $Z_n^m(x,y)$ then the phase ϕ may be described by a series of polynomials i.e.

$$\phi(x,y) = C_{00} + C_{01}Z_{01}(x,y) + C_{11}Z_{11}(x,y) + \ldots\ldots\ldots + C_{mn}Z_{mn}(x,y) + \ldots\ldots, \tag{19}$$

Once the phase is described in this manner then the derivatives of the phase can be easily determined from,

$$\frac{\partial \phi}{\partial x} = C_{01}\frac{\partial z_{01}}{\partial x} + C_{11}\frac{\partial z_{11}}{\partial x} + \ldots\ldots + C_{mn}\frac{\partial z_{mn}}{\partial x} + \ldots\ldots\ldots, \qquad (20)$$

with a similar expression for the y derivative. Eqn. (20) is then fitted to the wavefront slope data using a least squares method. This determines the complete wavefront slope.

3.3 Experimental Set Up

A block diagram of the experimental set up used is shown in Figure. 8. A laser beam from a Helium-Neon source (λ = 633nm) was passed through a telescopic lens system consisting of two lenses and onto an SLM liquid crystal display which was in reflective mode only. The first lens had a focal length of 50mm and the second 200mm. The laser beam therefore underwent a magnification of four to make its size big enough on the SLM screen width. The reflected beam with the aberration coefficients imprinted on it was then imaged onto the detector grid of a two dimensional Shack-Hartmann wavefront sensor using a 4f lens imaging system.

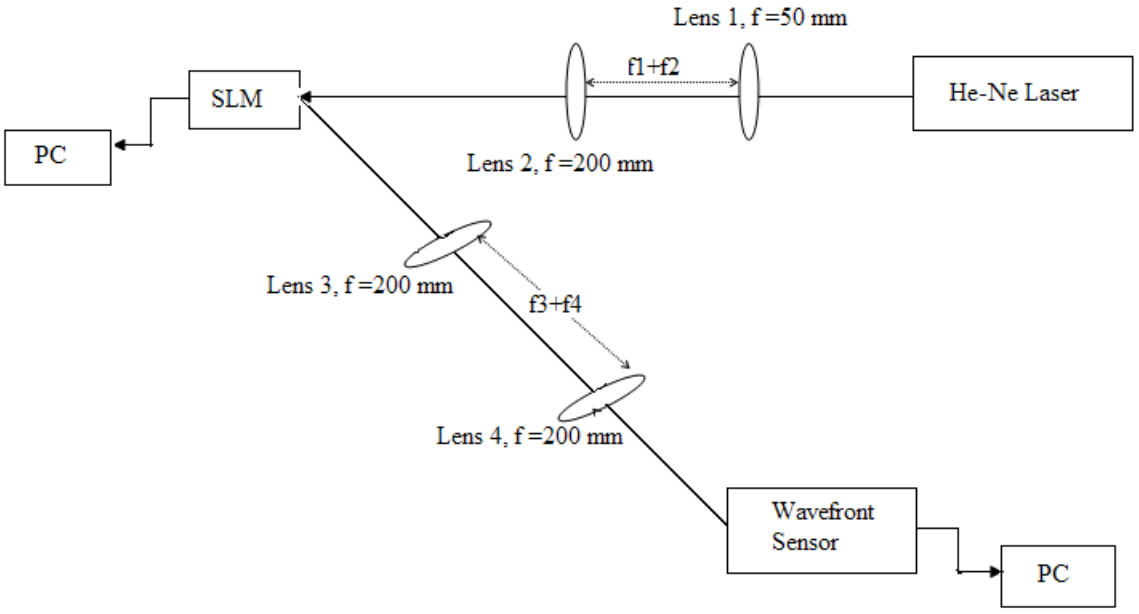

Figure. 8 A block diagram for measuring the focal length of a lens generating aberrations: PC- Computer, SLM- Spatial light modulator and *f*- focal length.

The sensor was connected to a computer which showed the wavefront properties e.g. phase and intensity distribution of the laser beam, together with the aberration coefficients fitted

into Zernike polynomials. Care was taken to make sure that the Zernike polynomials programmed onto the SLM agreed within reasonable error margin, with those measured by the sensor. This was achieved by using a calibration process. The experimental process was then carried out with coefficients between -3.1 and +3.1 λ of each aberration i.e. defocus, *x* and *y* astigmatism, *x* and *y* triangular astigmatism, *x* and *y* coma, *x* and *y* tilt and spherical aberration. To improve accuracy of the results, some twenty frames of each aberration measurement were acquired and averaged out by the sensor software.

Figures 9 through 13 shows examples of a 2D plot of the primary aberrations phase screens which were programmed onto the Spatial Light Modulator. The Zernike radius used was 1.44mm.

Figure 9 (a) 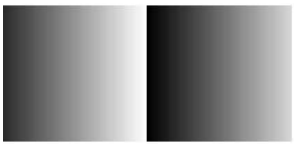

Figure 9 (b) 

Figure 10 (a) 

Figure 10 (b) 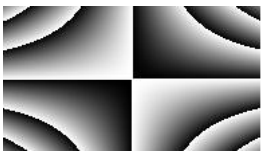

Figure 11 (a) 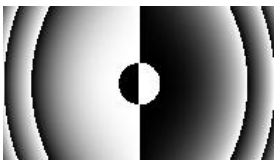

Figure 11 (b) 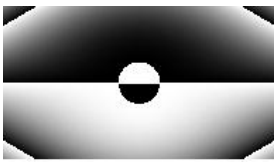

Figure 12 (a) 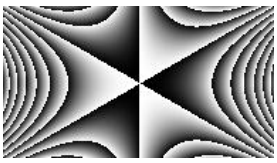

Figure 12 (b) 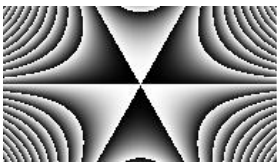

Figure 13 (a) 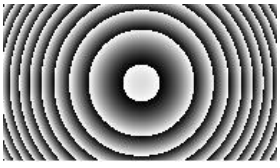

Figure 13 (b) 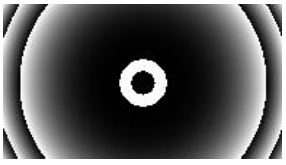

Figures 9 through 13 shows, 9 (a) X-Tilt for A = 0.5, d = 3, 9 (b) Y-Tilt for A = 0.5, d = 3, 10 (a) X-Astigmatism for A = 0.2, d = 3, 10 (b) Y-Astigmatism for A = 0.2, d = 3, 11 (a) X Coma for A = 0.01, d = 3, 11 (b) Y Coma for A = 0.01, d = 3, 12 (a) X-Triangular for A =

0.2, d = 3, 12 (b) Y-Triangular for A = 0.2, d = 3, 13 (a) Spherical Aberration for A = 0.001, d = 3 and 13 (b) Defocus for A = 0.2, d = 3.

CHAPTER FOUR

4.0 RESULTS AND DISCUSSIONS.

4.1 Derivation of the Tensor Formulation Used To Calculate Beam Size and Curvature

4.1.1 Cartesian Coordinates

The cartesian plane with a horizontal and vertical planes can be described using the variables *x* and *y*. Normalizing each variable with a square aperture of length *2a* gives new variables $x = x'/a$ and $y = y'/a$. This means that both x and y have a magnitude of 1 at the edge of the aperture and 0 at the centre. For a totally coherent laser beam, the beam size becomes a tensorial parameter that can be defined as a *2x2* matrix (Alda, 2003). This matrix involves the calculation of the moments of irradiance distribution in the plane of interest. The generalised beam size tensor is therefore given as;

$$w^2 = 4a^2 \begin{bmatrix} \begin{pmatrix} \langle x^2 \rangle & \langle xy \rangle \\ \langle xy \rangle & \langle y^2 \rangle \end{pmatrix} - \begin{pmatrix} \langle x \rangle \\ \langle y \rangle \end{pmatrix} \begin{pmatrix} \langle x \rangle & \langle y \rangle \end{pmatrix} \end{bmatrix}. \tag{21}$$

Since *a*, is the actual radius of the circular aperture, w^2 is a dimensional quantity. The vectors $\langle x \rangle$ and $\langle y \rangle$ represent mean values, defined in terms of the moments of the intensity distribution. They also describe any possible decentralization of the beam. The normalized moment used is;

$$\langle x^n y^m \rangle = \frac{\iint |\psi(x,y)|^2 x^n y^m \, dxdy}{\iint |\psi(x,y)|^2 \, dxdy}, \tag{22}$$

Where $\iint |\psi(x,y)|^2 \, dxdy = I(\psi)$ denotes the total irradiance of the beam. The second term of the matrix in Eqn. (21) involves the first-order moments that cancel only if the intensity distribution is centered with respect to the coordinate system used.

Any arbitrary laser field can be fitted with an average curvature, *R*. The term $\frac{w^2}{R}$ can be defined as:

$$\frac{w^2}{R} = -\frac{2\lambda a^2}{\pi I(\psi)} dxdy \, |\psi(x,y)|^2 \begin{bmatrix} (x - \langle x \rangle)\frac{\partial \phi}{\partial x} & (x - \langle x \rangle)\frac{\partial \phi}{\partial y} \\ (y - \langle y \rangle)\frac{\partial \phi}{\partial x} & (y - \langle y \rangle)\frac{\partial \phi}{\partial y} \end{bmatrix}, \tag{23}$$

where ϕ is the phase of the amplitude distribution and $\psi(x,y) = |\psi(x,y)|\exp[i\phi(x,y)]$. The phase term does not appear in the calculation of the beam size hence the beam size is independent of the beams aberrations.

4.1.2 Cylindrical Coordinates

Most laser beams, have a cylindrical geometry i.e. they have a circular cross section and propagate through a circular aperture. This implies that the equations in section 4.1.1 have to be converted into cylindrical coordinates. To do this a circular aperture of radius *a* is fitted inside the square one described in section 4.1.2, and shown in Figure. 14.

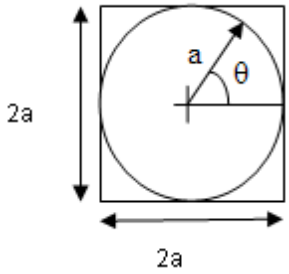

Figure. 14 Circular aperture of radius a, fitted inside a square aperture of length $2a$.

This means that Eqns. (21), (22) and (23) can be converted to cylindrical form and solved in the new aperture while maintaining the solutions for the basic laser beam parameters in *x* and *y* configurations.

Taking the main diagonal elements of Eqn. (23) and using $x = \rho Cos\theta$, $y = \rho Sin\theta$ and $\psi(x,y) = \psi(\rho,\theta)$ then $\frac{\partial}{\partial x} = Cos\theta\frac{\partial}{\partial\rho} - \frac{Sin\theta}{\rho}\frac{\partial}{\partial\theta}$ and $\frac{\partial}{\partial y} = Sin\theta\frac{\partial}{\partial\rho} + \frac{Cos\theta}{\rho}\frac{\partial}{\partial\theta}$ where $\rho \in [0\ 1]$ and $\theta \in [0\ 2\pi]$.

Therefore:

$$\left.\begin{aligned}\left(\frac{w^2}{R}\right)_x &= -\frac{2\lambda a^2}{\pi I(\psi)}\iint \rho d\rho d\theta\psi^2\left(\rho Cos\,\theta - \frac{a^2}{I(\psi)}\iint \rho d\rho d\theta\psi^2\rho Cos\,\theta\right)\left(Cos\,\theta\frac{\partial\rho}{\partial\theta} - \frac{Sin\,\theta}{\rho}\frac{\partial\rho}{\partial\theta}\right),\\ \left(\frac{w^2}{R}\right)_y &= -\frac{2\lambda a^2}{\pi I(\psi)}\iint \rho d\rho d\theta\psi^2\left(\rho Sin\,\theta - \frac{a^2}{I(\psi)}\iint \rho d\rho d\theta\psi^2\rho Sin\,\theta\right)\left(Sin\,\theta\frac{\partial\rho}{\partial\theta} + \frac{Cos\,\theta}{\rho}\frac{\partial\rho}{\partial\theta}\right).\end{aligned}\right\} \quad (24)$$

At the same time, the beam size main diagonal elements are given as:

$$w_x^2 = \frac{4a^2}{I(\psi)}\iint \rho d\rho d\theta \psi^2 \rho^2 Cos^2\theta - \left(\frac{2a^3}{I(\psi)}\iint \rho d\rho d\theta \psi^2 \rho Cos\,\theta\right)^2,$$

$$w_y^2 = \frac{4a^2}{I(\psi)}\iint \rho d\rho d\theta \psi^2 \rho^2 Sin^2\theta - \left(\frac{2a^3}{I(\psi)}\iint \rho d\rho d\theta \psi^2 \rho Sin\,\theta\right)^2. \qquad (25)$$

4.2 Analytical Computation

The cylindrical model presented in section 4.1.2 can be applied to a laser beam whose circular aperture has a Zernike radius *a*. To include the effects of truncation, the truncation parameter is defined as $\gamma = \frac{a}{w}$, where w is the beam size. The parameter will be used to analyze the effect of different aperture sizes on the propagated laser beam properties. In terms of the truncation parameter the electric field of a light beam can be described as;

$$E(\rho,\theta) = \left(\frac{2\gamma^2}{\pi a^2}\right)^{\frac{1}{4}} \exp(-\gamma^2\rho^2)\exp(i\phi(\rho,\theta)), \qquad (26)$$

where phase ϕ, is given in terms of the Zernike polynomials. According to Gaussian beam theory, beam radius w is defined as the size of two standard deviations of a Gaussian distribution. Any aperture radius, with respect to the beam size is important in that it shows the amount of diffraction due to the aperture. Large aperture implies that most of the energy of the beam goes through, therefore the distribution is a pure Gaussian beam, and on the other hand a small aperture implies that the beam is uniform. The first case is known as a hard aperture while the latter as a soft aperture. For the laser beam, the radius of curvature in both the horizontal and vertical planes can be deduced from Eqn. (24) by substituting in the value of field Eqn. (26) and phase Eqn. (10) and dividing by beam size as defined by Eqn. (25). This then becomes,

$$\frac{1}{R_x} = \frac{2\lambda}{a^2}\left(-2\sqrt{3}A_{20} - \sqrt{6}A_{22} + 6\sqrt{5}\left(1 - \frac{2}{\gamma^2} + \frac{4\gamma^2}{e^{2\gamma^2} - 1 - 2\gamma^2}\right)A_{40}\right),$$

$$\frac{1}{R_y} = \frac{2\lambda}{a^2}\left(-2\sqrt{3}A_{20} + \sqrt{6}A_{22} + 6\sqrt{5}\left(1 - \frac{2}{\gamma^2} + \frac{4\gamma^2}{e^{2\gamma^2} - 1 - 2\gamma^2}\right)A_{40}\right). \qquad (27)$$

From Eqn. (27), it can be seen that the curvature of the field is directly proportional to individual amounts of defocus, x-astigmatism and spherical aberration. Curvature is represented by $K = \frac{a}{\lambda f}$.

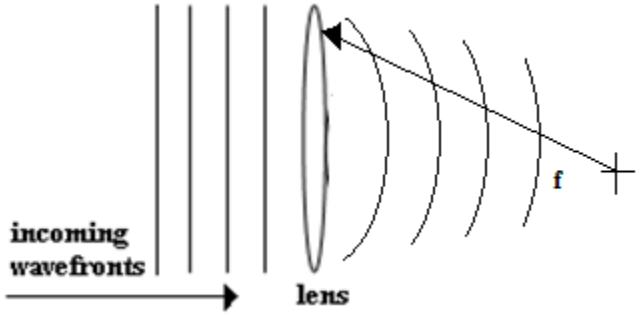

Figure. 15: Wavefronts converging to a point of distance equal to a lens focal length *f*.

If a positive lens of focal length *f* is placed in the path of a propagating beam such that the waist of the beam is just in front of the lens, the curvature at that particular point will be zero, (see Figure. 15). Using the lens equation $\frac{1}{R_f} = \frac{1}{R_i} + \frac{1}{f}$ where R_i and R_f denotes the curvature of the field in front and behind the lens respectively, then $\frac{1}{R_i} = 0$ and $\frac{1}{R_f} = \frac{1}{f}$.

This implies that the general focal length is given by;

$$\left.\begin{aligned} \frac{1}{f_x} &= \frac{2\lambda}{a^2}\left(-2\sqrt{3}A_{20} - \sqrt{6}A_{22} + 6\sqrt{5}\left(1 - \frac{2}{\gamma^2} + \frac{4\gamma^2}{e^{2\gamma^2} - 1 - 2\gamma^2}\right)A_{40}\right), \\ \frac{1}{f_y} &= \frac{2\lambda}{a^2}\left(-2\sqrt{3}A_{20} + \sqrt{6}A_{22} + 6\sqrt{5}\left(1 - \frac{2}{\gamma^2} + \frac{4\gamma^2}{e^{2\gamma^2} - 1 - 2\gamma^2}\right)A_{40}\right). \end{aligned}\right\} \quad (23)$$

Eqn. (28) gives the theoretical formulation for calculating the focal length in both x and y axis given a lens generating aberrations. The aberrations are seen to be inversely related to the focal lengths. The formulation also clearly shows that the only aberrations which have an effect on the focal length and hence on the imaging properties of a lens are defocus, x-astigmatism and spherical aberration.

4.3 Special Cases

(a) For a hard aperture i.e. very large γ, the terms $4\gamma^2\left(e^{2\gamma^2}-1-2\gamma^2\right)^{-1}$ and $\frac{2}{\gamma^2}$ approaches zero. This means that the Gaussian source approximates a uniform field, therefore the lens power becomes

$$\left.\begin{aligned}\frac{1}{f_x}&=\frac{2\lambda}{a^2}\left(-2\sqrt{3}A_{20}-\sqrt{6}A_{22}+6\sqrt{5}A_{40}\right),\\ \frac{1}{f_y}&=\frac{2\lambda}{a^2}\left(-2\sqrt{3}A_{20}+\sqrt{6}A_{22}+6\sqrt{5}A_{40}\right).\end{aligned}\right\} \qquad (29)$$

(b) In the case of a soft aperture i.e. if the aperture radius a is greater than 2ω or $\gamma \geq 2$, then the term $4\gamma^2\left(e^{2\gamma^2}-1-2\gamma^2\right)^{-1}$ approaches zero. Lens power becomes;

$$\left.\begin{aligned}\frac{1}{f_x}&=\frac{2\lambda}{a^2}\left(-2\sqrt{3}A_{20}-\sqrt{6}A_{22}+6\sqrt{5}\left(1-\frac{2}{\gamma^2}\right)A_{40}\right),\\ \frac{1}{f_y}&=\frac{2\lambda}{a^2}\left(-2\sqrt{3}A_{20}+\sqrt{6}A_{22}+6\sqrt{5}\left(1-\frac{2}{\gamma^2}\right)A_{40}\right).\end{aligned}\right\} \qquad (30)$$

4.4 Theoretical Results

From the theoretical model developed in section 4.2, Eqn. (28), the difference in the two set of equations can be observed in the horizontal and vertical axes of the three aberrations i.e. defocus, X- astigmatism and spherical aberrations. From equation (28), for a laser beam to converge, the focal length must be positive. This means that defocus (A_{20}) must always be negative for a positive lens. A positive value would do the opposite. On the other hand X-astigmatism has different polarities in the two planes i.e. one is positive and the other negative. This has the effect of splitting the focal plane in the two axes; the axis with the positive value shifting its plane forward in the direction of propagation, while the other backwards, both by the same distance. Spherical aberration is the only one whose effect on the lens focal length is not constant since its coefficient is dependent on the truncation parameter γ. It converges the beam for $\gamma < 1.15931$ and diverges it when $\gamma > 1.15931$. For $\gamma = 1.15931$ spherical aberration has no effect on the lens' focal length since its zero i.e. $1-\frac{2}{\gamma^2}+\frac{4\gamma^2}{e^{2\gamma^2}-1-2\gamma^2}=0$.

Figure 16 shows four pairs of graphs, one for each pair of *x* and *y* axis for γ = 0.3, 1, 2 and 3. The values of γ are chosen randomly such that two values i.e. 0.3 and 1 are less than 1.15931 while the other two i.e. 2 and 3 are greater than 1.15931. On each graph it is assumed that the other two primary aberrations are zero.

(a) $\gamma = 0.3$

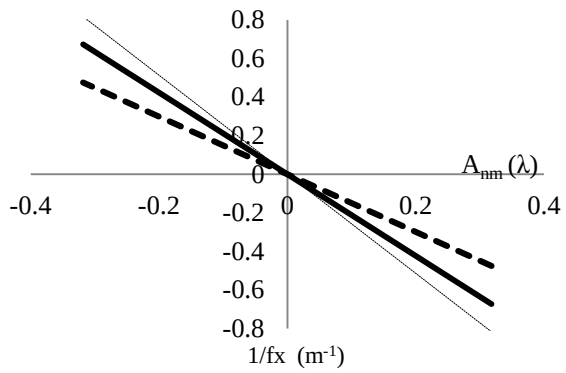

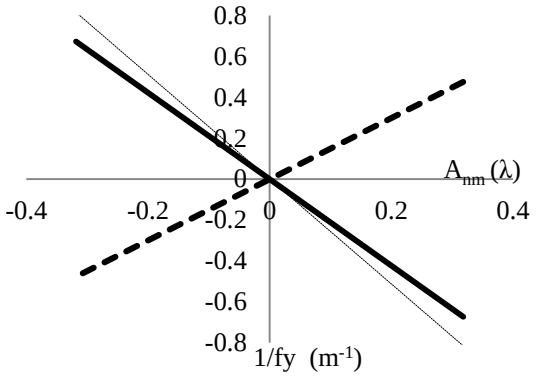

(b) $\gamma = 1$

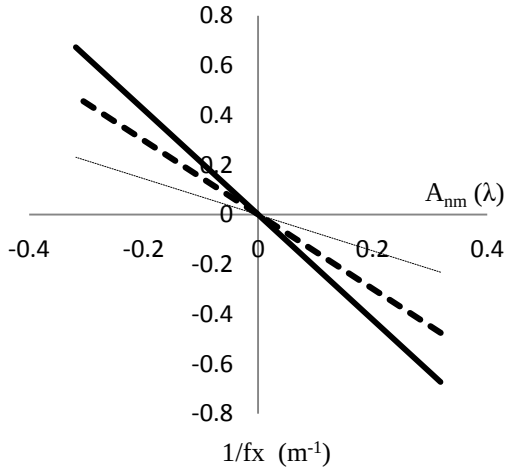

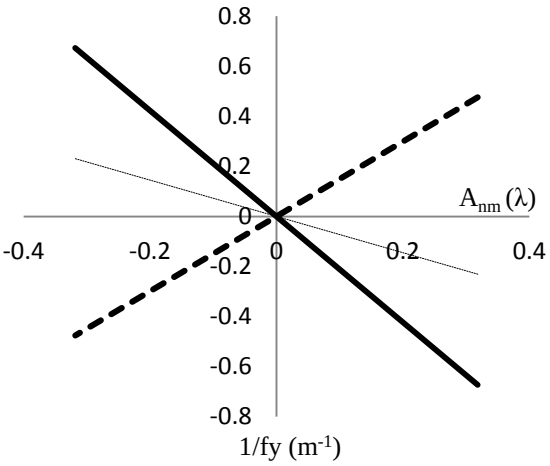

(c) $\gamma = 2$

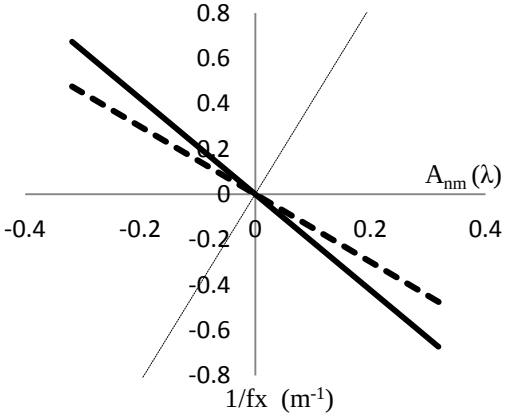

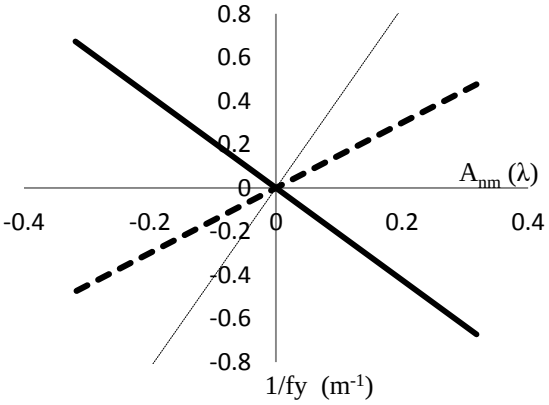

(d) $\gamma = 3$

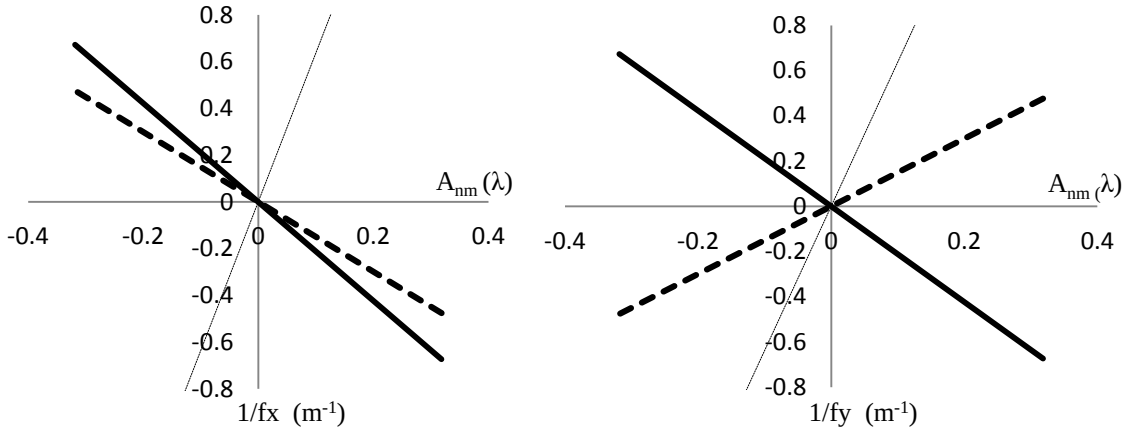

Figure 16 Generalised focal length variation with individual amounts of defocus (—), x-astigmatism (- - -) and spherical aberration (.....) in the x and y axis for γ = 0.3, 1, 2 and 3.

4.5 Experimental Results

4.5.1 Calibration Results

The calibration procedure for the SLM is achieved by an interferometric measurement of two coherent beams with one modulated in phase by the SLM, after which the programmed gray scale is assigned to a particular phase value from 0 (white) to 2π (black). This particular SLM (Pluto SLM) has a poor response at low phase values, as shown in Figure 17, where the calibration curve has a "threshold" phase value prior to becoming responsive.

Since each Zernike coefficient is a measure of how much each aberration contributes to the laser beam wavefront, care was therefore taken to ensure that the Zernike polynomial system used in both the SLM phase patterns and Shack-Hartmann sensor software matched. Therefore the wavefront sensor was calibrated using the phase only SLM. First a reference frame was created without a phase pattern being loaded onto the SLM. This was done to subtract the effects of the curvature of the screen and remove the aberrations in the laser beam. Since the plots are mod-2π, the Zernike coefficient programmed in each case is the coefficient of each polynomial divided by 2π. Various coefficients of each of the primary Zernike polynomials were recorded onto the SLM. The nominal coefficients ranged from -2 to 2, in steps of 0.2. This means that the nominal root mean square (*rms*) value of Zernike coefficients ranged from $-2/2\pi$ to $2/2\pi$ waves, in steps of $0.2/2\pi$, or -0.318 to 0.318 waves, in steps of 0.0318. For each phase pattern, at least 10 frames were measured by the sensor from

which an average was acquired. Plots for each aberration were prepared showing the relationship between the SLM values on the *x*-axis and the corresponding sensor values on the *y*-axis. The aberrations calibrated for are all the primary aberrations except *x*- and *y*-tilt. Figure 17 shows the calibration curve for defocus. Only the curve for defocus is shown since all the curves of each aberration calibrated are identical.

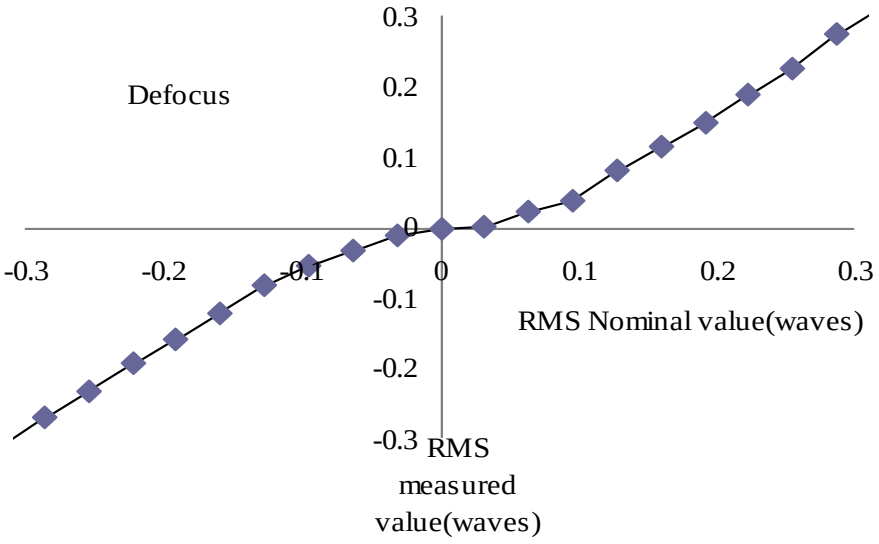

Figure.17 Calibration plot of the primary aberrations.

4.5.2 Data Collection

The measurements taken by the class 2D wavefront sensor included phase parameters in the form of Zernike coefficients and laser beam parameters in the form of beam quality M^2, beam size w, divergence θ and waist location Z_0. This meant that the experiment was able to ascertain any phase changes to the accompanying change in the other parameters. The SLM was therefore used as a lens since the primary aberrations with selected coefficients were programmed onto it. The experimental data are presented in Appendix A, (Tables A1-A10). From the data tables, radius of curvature was calculated using the formula below,

$$R = z\left(1+\left(\frac{w^2\pi}{z\lambda M^2}\right)^2\right),$$

where λ, is the wavelength of the laser beam used. The focal length was calculated from,

$$f = \frac{1}{\left(\frac{1}{R_r} - \frac{1}{R_{x,y}}\right)},$$

where R_r is the reference radius of curvature and $R_{x,y}$ is the radius of curvature in the x and y axis, respectively.

4.4.3 Data Analysis

The control Zernike coefficients in the theoretical model were replaced with respective experimental coefficients so as to get the correct theoretical curve. This is what was used to compare with the experimental results. From the data collected in Tables A1 – A10, the value of the lens power i.e. $\frac{1}{f}$ was calculated and the graphs of $\frac{1}{f}$ against each aberration for both the experimental results and the theoretical model were plotted on the same axis for comparison purposes. The results for each of the third order primary aberrations are presented in Figures. 18(a) – 18(d).

(a) Defocus aberration.

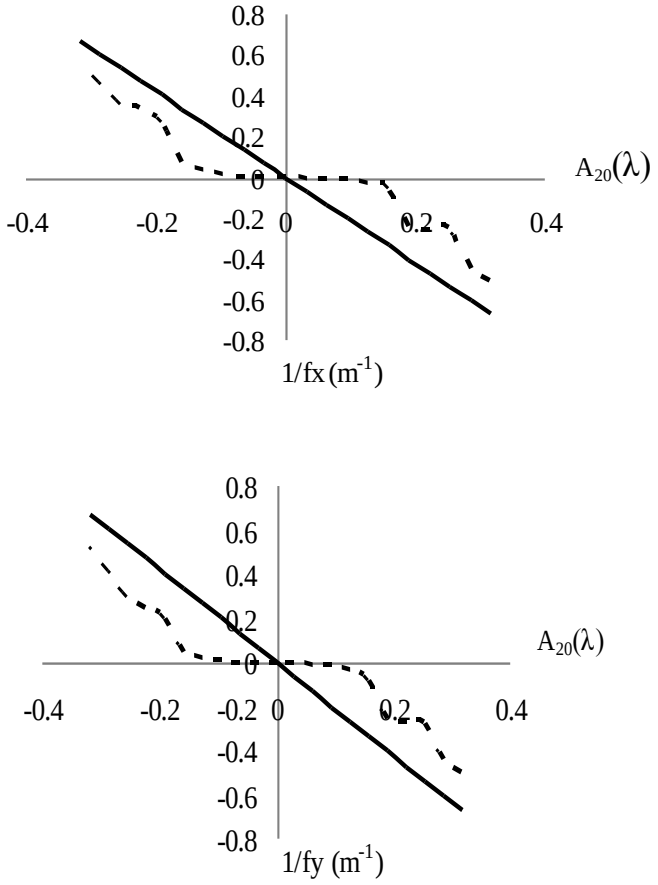

Figure 18 (a). Curvature dependence for both theoretical (——) and experimental (·····) results on defocus.

(b) X-Astigmatism aberration.

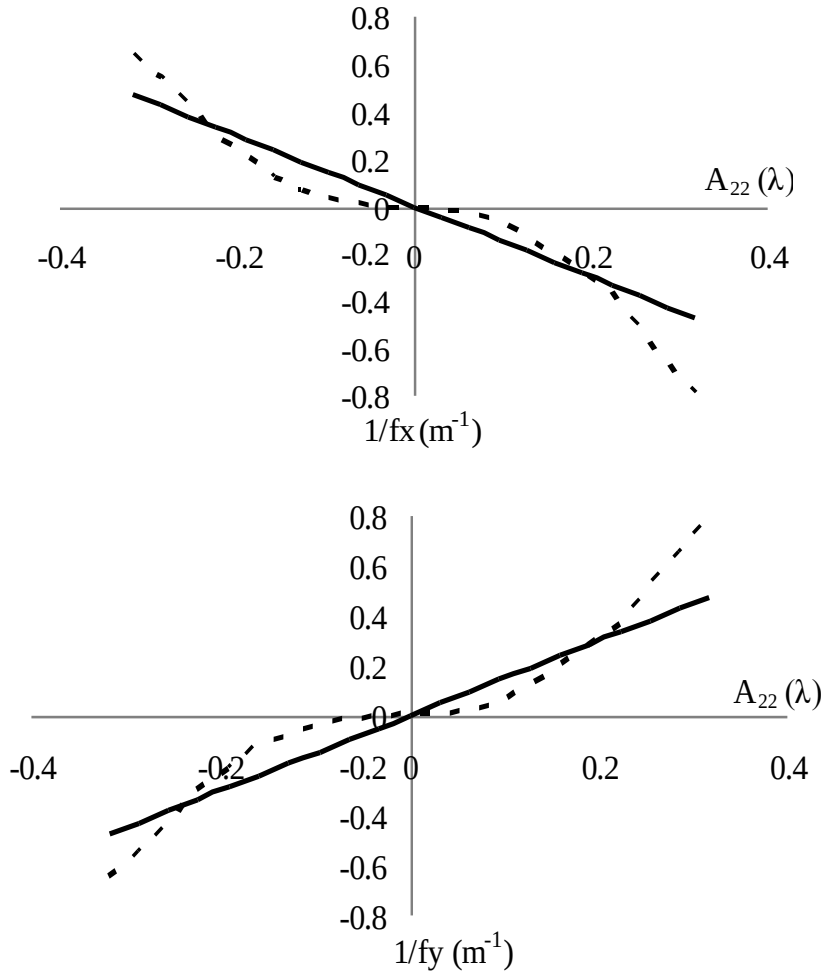

Figure 18 (b). Curvature dependence for both theoretical (—) and experimental (·····) results on X-Astigmatism aberration.

(c) Spherical aberration.

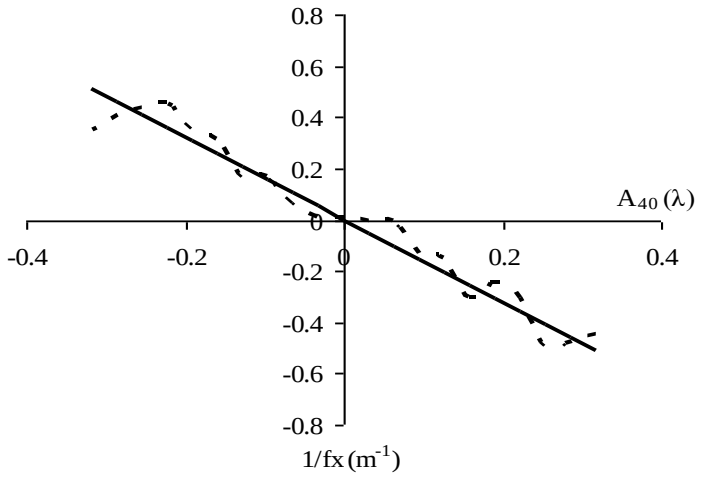

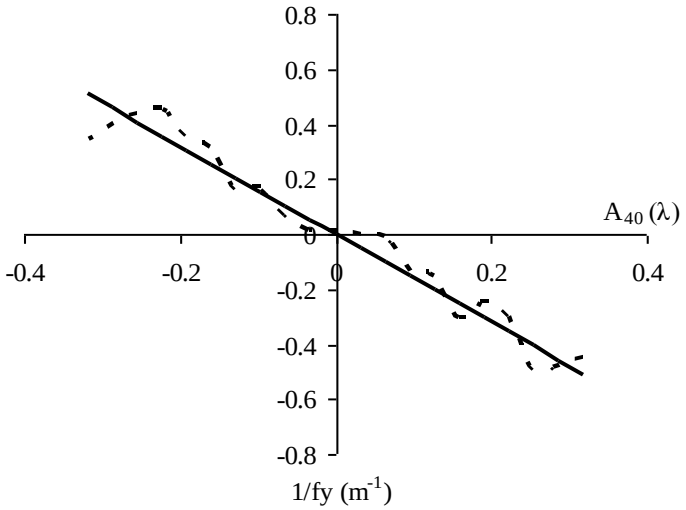

Figure 18 (c). Curvature dependence for both theoretical (—) and experimental (·····) results on Spherical aberration.

(d) The rest of the primary aberrations.

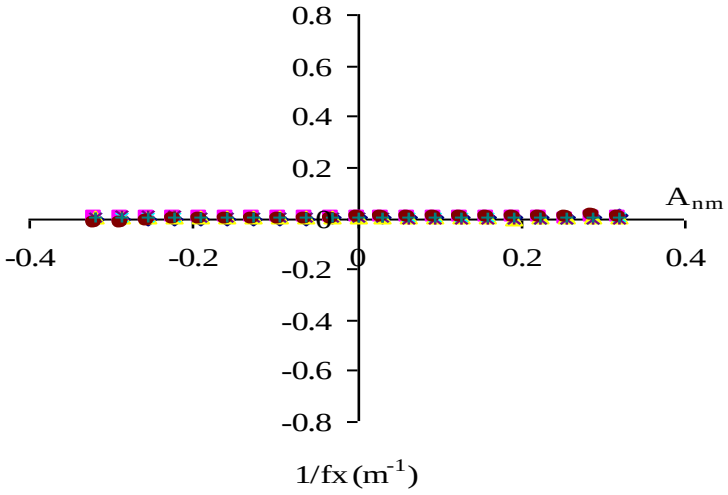

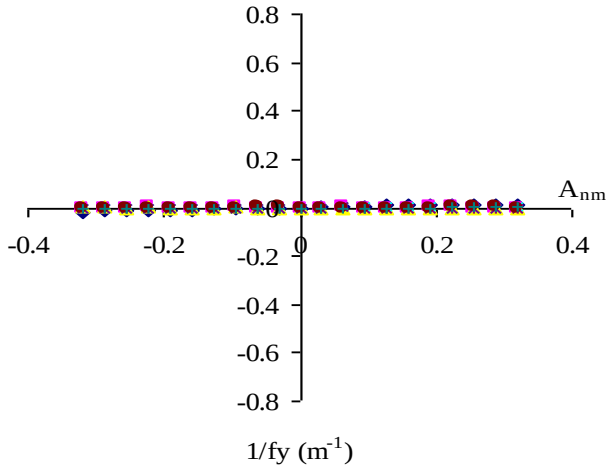

Where;

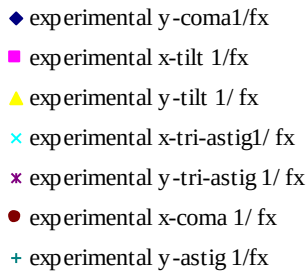

Figure.18 (d) Curvature dependence for both theoretical (——) and experimental (·····) results on other primary aberrations.

Figures 18 (a) and (c) show the results for defocus and spherical aberration respectively, which are the same in both axes. The model agrees well with the experimental results with the exception that the experimental results exhibit no phase response at the origin (since no phase was imparted to the device). This is as a result of calibration of the SLM which accounts for the deviation of the theory and experimental data in all the graphs. The data plotted followed the same trend as shown in the calibration curve of the SLM in Figure 17. In Figure 18 (b) there are two focal planes for each amount of *x*-astigmatism. Figure 18 (d) shows that the focal length is constant as different amounts of the aberrations are added thus confirming the theoretical model formulated in section 4.1.2.

4.6 Discussions

The theoretical model derived in section 4.2 gives a formula that allows any aberrated lens to be described and equated to a single focal length, regardless of the type or origin of the aberrations. Our posed problem is how to use the deformed, cracked or imperfect lenses in our laboratories, research institutions as well as in industries. It may not be easy to say what impact these deformations may have on a particular optical system without the details of the lens design parameters, however, the analysis presented in this thesis readily allows for the assessment of the error in the focal length given some contribution from one or more aberrations. From the theoretical results shown in Figure 16, the effect of varying the truncation parameter has been presented. Out of the three aberrations i.e. spherical, x-astigmatism and defocus, only spherical aberration effect on the focal length is not constant. It converges the beam for $\gamma < 1.15931$ and diverges it when $\gamma > 1.15931$. For $\gamma = 1.15931$ spherical aberration has no effect on the lens' focal length since its zero.

The data collection tables given in the Appendix A section outlines different lens imaging properties, most important being the divergence and beam quality of the laser beam after it has passed through an aberrated lens. Taking the x-plane it can be seen that generally, divergence increases with increase in the aberration coefficients. If we consider the three aberrations that have an effect on the lens focal length then for aberration coefficient -2, divergence for spherical aberration (0.4785) is greater than that of defocus aberration (0.4449) and x-astigmatism aberration (0.237). The same trend applies to all the other aberration coefficients. It is also observed that for aberration coefficient -2, the beam quality in the x- plane deteriorates more for spherical aberration (13.755) followed by x-astigmatism (2.216) and lastly defocus (1.397). The same trend applies to the rest of the aberrations both in the x and y planes.

The predicted model has been experimentally verified by introducing the aberrated lens in the form of digital holograms shown in Figures 9 - 13. The results confirm the model quite satisfactorily except for spherical and x-astigmatism aberrations. This is because all the measurements were made in the plane where Seidel defocus is zero. To correct for this, extra defocus would have to be added to the experimental results. The formulae for doing this are derived in Appendix B. After the corrections for defocus aberration which is inherent in every lens, the experimental results follows the same trend that is predicted by the theoretical model as seen in Figure 18.

CHAPTER FIVE

5.0 CONCLUSION AND RECOMMENDATIONS

5.1 Conclusion

According to the results only astigmatism was adversely affected in that two separate astigmatic focal surfaces were formed to correspond to the tangential and sagittal conjugates. This blurred the image even more. In the case of spherical aberration, the images formed on the two focal planes appeared curved. For coma, distortion and defocus, the image formed were not changed by the presence of field curvature aberration, since the image plane formed by the respective aberrations was already curved.

A model for calculating the focal length given an aberrated lens has been presented. This approach has led to a solution expressed as a function of low-order Zernike polynomials, which corresponds to third order aberrations. It has been shown that there are three primary Zernike coefficients related to defocus, spherical and x-astigmatism which should be known if the focal length of an aberrated lens is to be determined. These three aberrations individually or collectively are inversely related to the focal length and are the only ones which require defocus to balance them. This is a possible formulation which can be used for any aberrated lens of any size focussing a Gaussian beam of any size with an arbitrary choice of aperture.

5.2 Recommendations

- More studies should be carried out on this subject using higher order aberrations.
- The calibration procedure for the SLM (Pluto) should be improved such that the poor response at low phase values does not occur. Since this tends to have an impact on the results.

REFERENCES

Alda J., Alonso J. and Bernabeu E., (1997), *Characterization of aberrated laser beams*, Optical Society of America, Vol. **(A)**. **14**, Pg 2737-2747.

Alda J., (2003), *Laser and Gaussian Beam Propagation and Transformation*, Encyclopedia of Optical Engineering, Pg 999-1013.

Bezdid'ko S. N., (1974), *The use of Zernike polynomials in optics*, Soviet Journal of Optical Technology, Vol. **41**, Pg 425-429.

Born M. and Wolf E., (1999), *Principles of Optics*, Cambridge University Press, Cambridge 7th ed. Pg 228-240.

Dai G. M., (2008), *Wavefront Optics for Vision Correction*, SPIE Press. Pg 1-5.

Francis A. J. and Harvey E., (1976), *Fundamentals of Optics*, McGraw Hill, 4th ed. Pg 149-182.

Hopkins H. H., (1950), *Wave Theory of Aberrations*, Oxford University Press London.

James C. W. and Katherine C., (1992), *Basic Wavefront Aberration Theory for Optical Metrology,* Applied Optics. and Optical Engineering. Vol. **11**, Academic Press Inc. Pg 1-53.

Jason D. S., (2010), *Numerical Simulation of Optical Wave Propagation with examples in MATLAB*, SPIE Press. Pg 65-84.

Karim M. A., (1990), *Electro-optical Devices and System,* (PWS-KENT) Publishing Company, Boston, Pg 200-248.

Konforti N., Marom E. and Wu S. T., (1988), *Phase-only modulation with twisted nematic liquid-crystal spatial modulators*, Optical Letter, Vol. **13**, Pg 251-253.

Larry C. A. and Ronald L. P., (2005), *Laser Beam Propagation through Random Media*, SPIE Press, 2nd ed. Pg 15-50.

Mahajan V. N., (1991), *Aberration Theory Made Simple*, SPIE Press, Pg 69-80.

Mahajan V. N., (1994), *Zernike Circle Polynomials and Optical Aberrations of Systems with Circular Pupils*, Engineering and Laboratory Notes, Pg 8121-8124.

Mahajan V. N., (1998), *Optical Imaging and Aberrations Part 1: Ray Geometrical Optics*, SPIE Press, Pg 131-160.

Mahajan V. N., (2003), *Zernike Polynomials and Aberration balancing in Current Developments in Lens Designs and Opt Eng*, SPIE Proceedings, Vol. **5173**, Pg 1-16.

Mahajan V. N., (2007), *Zernike Polynomials and Wavefront Fitting*, in Optical Shop Testing, D. Malacara, Wiley Inc, 3rd ed, Pg 498-530.

Neal D. R., Alford W. J. and Gruetzner J. K., (1996), *Amplitude and Phase Beam Characterization using a two-dimensional Wavefront Sensor*, SPIE Proceedings, Vol. **2870**, Pg 72-82.

Neal D. R., Copland J. and David N., (2002), *Shack-Hartmann Wavefront Sensor Precision and Accuracy*, SPIE Proceedings, Vol. **4779**, Pg 148-160.

Neal D. R., Armstrong D. J. and Turner W. T., (1997), *Wavefront sensors for control and process monitoring in optics manufacture*, SPIE Proceedings, Vol. **2993**, Pg 211-220.

Noll R. J., (1976), *Zernike Polynomials and Atmospheric Turbulence*, Journal of Optical Society of America, Vol. **73**, Pg 207-211.

Pluto SLM retrieved from: http://www.holoeye.com/spatial_light_modulators_pluto.html, 29th, March 2012, 18:41 pm.

Robert E. F., Biljana T. G. and Paul R. Y., (2000), *Optical System Design*, McGraw Hill, 2nd ed. Pg 35-45.

Ruff J. A. and Siegman A. E., (1993), *Measurement of beam Quality Degradation due to Spherical Aberration in a Simple Lens*, Optical Quantum Electronics, Vol. **26,** Pg 629-632.

Siegman A. E., (1993), *Analysis of Laser Beam Quality Degradation caused by Quartic Phase Aberrations*, Applied Optics, Vol. **32**, Pg 5893-5091.

Singh R. K., Senthilkumaran P. and Singh K., (2007), *The effect of astigmatism on the diffraction of a vortex carrying beam with a Gaussian background,* Journal of Optics, Vol **A (9)**, Pg 543–554.

Spherical aberration of a concave spherical lens, retrieved from: http://www.telescope-optics.net/spherical1.htm, 13th January, 12:30 pm.

Sudarshan E.C.G., Simon R. and Mukunda N., (1983), *Paraxial wave optics and relativistic front description. 1. The scalar theory,* Physical Review, Vol. **A (28)**, Pg 2921-2932.

Tripoli N, M. A., (2002), *The Zernike Polynomials,* Dept. of Ophthalmology, University of North Carolina at Chapel Hill, NC, U.S.A. Pg 1-15.

Wada A., Ohminato H., Yonemura T., Miyamoto Y. and Takeda M., (2005), *Effect of comatic aberration on the propagation characteristics of the Laguerre–Gaussian beams*, Optical Review, Vol. **12**, Pg 451–455.

Wang J. Y. and Markey J. K., (1977), *Modal compensation of atmospheric turbulence phas*e *distortion,* Journal of Optical Society of America, Vol. **68**, No.1, Pg 78-87.

Wavefornt sciences CLASS 2D Shack-Hartmann wavefront sensor, retrieved from: http://www.wavefrontsciences.com/clas_2d.html , 29th, March 2012, 18:41 pm.

Welford W. T., (1974), *Aberrations of the Symmetrical Optical System*, Academic Press, New York.

Wolfram Research Inc., (2007), *Mathematica Version 6.0*, Champaign Illinois.

APPENDIX A

The primary aberrations shown in Table 2 section 2.4, can be programmed on a spatial light modulator (SLM) using a Wolfram Mathematica program code (Wolfram research Inc., 2007) shown below to give several phase screens by adjusting the values of Zernike coefficient *A* which is in radians and *d*, which shows the scaling used to specify the Zernike circle for each aberration. The command used is $Mod\,2\pi$, since the liquid crystal display in the SLM works with phase shift from 0 to 2π . We therefore calculate the remainder after dividing the selected Zernike coefficient by 2π . This means that the actual coefficient being programmed is the nominal coefficient, say A/2π .

```
n = 1;
m = 1;
ρ = sqrt[x^2 + y^2];
θ = ArcTan[x, y];
R[n_, m_, ρ] := ZernikeR[n, m, ρ];
φ[n_, m_, ρ_, θ_] := A * Sqrt[2(n + 1)/(1 + Kronecker Delta[m, 0])] R[n_, m_, ρ] * Cos[m * θ];
A = 0.12;
w = 8.64; (*LCDscreenwidth*)
d = 3;
R_z = w / (2 * d) "mm − RadiusoftheZernikecircle"
"x − tilt"
DensityPlot[Mod[φ[n, m, ρ, θ], 2 * π], {x, −d*16/9, d*16/9}, {y, −d, d}, PlotRange → {{−d*16/9, d*16/9},
{−d, d}}, PlotPoints → 100, Frame → False, ColorFunction → GrayLevel, ImageSize → {{0,1920},
{0,1080}}, AspectRatio → 9/16]
```

Fig A1: A Mathematica program for creating an x-tilt phase screen on the SLM.

Tables A1 through A10 shows the data collected for the various primary aberrations.

Table A1: Data for defocus aberration.

Aberration coefficients	Beam Quality $(M^2)_x$	Beam Quality $(M^2)_y$	Divergence, θx	Divergence, θy	Waist location, Z_x	Waist location, Z_y
-2	1.397	1.368	0.4449	0.4486	-1.218	-1.246
-1.8	1.315	1.34	0.3902	0.4012	-1.34	-1.351
-1.6	1.287	1.218	0.3254	0.3421	-1.774	-1.806
-1.4	1.376	1.319	0.2833	0.2966	-1.698	-1.72
-1.2	1.286	1.343	0.2287	0.245	-1.787	-1.729
-1	1.194	1.22	0.1776	0.1999	-3.057	-2.828
-0.8	1.185	1.204	0.1334	0.1455	-3.455	-3.359
-0.6	1.264	1.302	0.0727	0.0904	-3.024	-3.322
-0.4	1.217	1.267	0.0366	0.054	-2.258	-2.843
-0.2	1.148	1.18	0.0025	0.025	-0.102	-0.887
0	1.133	1.15	-0.0097	0.0034	0.382	0
0.2	1.193	1.21	-0.0181	-0.0137	0.83	0.834
0.4	1.243	1.34	-0.0657	-0.0506	2.867	0
0.6	1.239	1.371	-0.1111	-0.0949	3.847	2.955
0.8	1.242	1.335	-0.1518	-0.1396	3.437	3.51
1	1.237	1.441	-0.215	-0.1911	2.801	2.874
1.2	1.27	1.434	-0.2697	-0.243	1.753	1.897
1.4	1.241	1.443	-0.3219	-0.2942	1.607	1.723
1.6	1.231	1.446	-0.3683	-0.347	1.574	1.613
1.8	1.236	1.398	-0.4177	-0.4015	1.362	1.382
2	1.269	1.315	-0.4745	-0.4512	1.204	1.26

Table A2: Data for x-astigmatism aberration.

Aberration coefficients	Beam Quality $(M^2)_x$	Beam Quality $(M^2)_y$	Divergence, θx	Divergence, θy	Waist location, Z_x	Waist location, Z_y
-2	2.216	8.983	0.2937	-0.3058	-1.637	0
-1.8	2.132	7.871	0.2609	-0.2709	-1.746	0
-1.6	1.999	6.995	0.2289	-0.2367	-1.93	0
-1.4	1.897	5.995	0.1923	-0.203	-2.149	0
-1.2	1.767	5.13	0.1626	-0.1702	-2.397	0
-1	1.548	3.935	0.117	-0.1282	-2.72	0
-0.8	1.373	3.134	0.0877	-0.0979	-2.97	0
-0.6	1.227	2.073	0.0543	-0.0599	-2.829	0
-0.4	1.239	1.392	0.0168	-0.0251	-1.271	0
-0.2	1.154	1.201	-0.0031	-0.0019	0.317	0.054
0	1.141	1.194	-0.0184	0.0041	1.442	0
0.2	1.188	1.359	-0.0242	0.0204	1.703	0
0.4	1.232	1.667	-0.046	0.0417	2.737	0
0.6	1.387	2.212	-0.0739	0.0732	3.258	0
0.8	1.548	3.137	-0.1175	0.1033	3.055	0
1	1.645	3.965	-0.1468	0.1355	2.749	0
1.2	1.732	5.176	-0.1865	0.1761	2.48	0
1.4	1.884	5.979	-0.2179	0.2108	2.189	0
1.6	2.034	6.944	-0.2548	0.2414	1.902	0
1.8	2.338	8.133	-0.3027	0.28	1.621	0
2	2.259	8.81	-0.3199	0.304	1.571	0

Table A3: Data for y- astigmatism aberration.

Aberration coefficients	Beam Quality $(M^2)_x$	Beam Quality $(M^2)_y$	Divergence, θx	Divergence, θy	Waist location, Z_x	Waist location, Z_y
-2	4.819	8.983	-0.0044	-0.0076	0.035	0.047
-1.8	4.253	7.871	-0.0037	-0.0039	0.048	0.055
-1.6	3.829	6.995	-0.0047	0.0001	0.062	0.01
-1.4	3.224	5.995	-0.0054	-0.0006	0.111	0.025
-1.2	2.743	5.13	-0.0081	0.0007	0.212	-0.003
-1	2.383	3.935	-0.0146	0.0053	0.488	-0.097
-0.8	1.923	3.134	-0.014	0.0028	0.711	-0.185
-0.6	1.615	2.073	-0.0132	0.0074	0.813	-0.007
-0.4	1.364	1.392	-0.0172	0.0089	0.438	0
-0.2	1.261	1.201	-0.0153	0.0068	0.963	0
0	1.138	1.194	-0.0192	0.0039	1.372	0
0.2	1.192	1.359	-0.0116	0.0068	1.041	0
0.4	1.343	1.667	-0.0121	0.0069	0.668	0
0.6	1.549	2.212	-0.0185	0.0073	1.147	0
0.8	1.994	3.137	-0.0157	0.012	0.683	-0.006
1	2.408	3.965	-0.0155	0.0129	0.479	-0.015
1.2	2.86	5.176	-0.0223	0.0112	0.415	-0.007
1.4	3.439	5.979	-0.0133	0.0196	0.227	-0.008
1.6	3.836	6.944	-0.018	0.0201	0.208	-0.011
1.8	4.501	8.133	-0.0239	0.0201	0.193	0
2	4.821	8.81	-0.0251	0.0212	0.159	0

Table A4: Data for x- triangular astigmatism aberration.

Aberration coefficients	Beam Quality $(M^2)_x$	Beam Quality $(M^2)_y$	Divergence, θx	Divergence, θy	Waist location, Z_x	Waist location, Z_y
-2	5.981	6.322	0.0053	-0.0358	0.001	0.002
-1.8	5.641	5.787	0.0135	-0.0326	0	0
-1.6	4.828	4.962	0.0074	-0.0313	-0.043	0
-1.4	4.324	4.364	0.0112	-0.0315	-0.077	0
-1.2	3.462	3.674	0.003	-0.0227	-0.035	0.02
-1	2.839	2.965	-0.001	-0.0138	0.02	0.076
-0.8	2.246	2.346	-0.0017	-0.0135	0.082	0.137
-0.6	1.656	1.814	-0.0084	-0.0077	0.433	0.377
-0.4	1.39	1.379	-0.0045	-0.0035	0.2	0.028
-0.2	1.218	1.245	-0.0134	0.0069	0.671	0
0	1.14	1.196	-0.0184	0.0045	1.184	0
0.2	1.248	1.316	-0.0138	0.0107	0.554	0
0.4	1.538	1.417	-0.0216	0.0075	0.745	0
0.6	2.099	1.718	-0.0238	0.0157	0.529	0
0.8	2.666	2.19	-0.0296	0.0169	0.525	0
1	3.225	2.811	-0.0342	0.0242	0.385	0
1.2	4.18	3.629	-0.0376	0.0242	0.295	0
1.4	4.821	4.338	-0.0423	0.0233	0.251	0
1.6	5.418	4.866	-0.0465	0.0288	0.163	0
1.8	6.079	5.531	-0.0559	0.0291	0.209	0
2	6.68	6.018	-0.0613	0.0331	0.179	0

Table A5: Data for y- triangular astigmatism aberration.

Aberration coefficients	Beam Quality $(M^2)_x$	Beam Quality $(M^2)_y$	Divergence, θx	Divergence, θy	Waist location, Z_x	Waist location, Z_y
-2	6.348	6.547	0.0501	-0.079	-0.131	0
-1.8	5.619	5.789	0.0462	-0.0699	-0.203	0
-1.6	5.054	5.232	0.0352	-0.0592	-0.169	0
-1.4	4.331	4.54	0.0322	-0.0507	-0.162	0
-1.2	3.605	3.765	0.0277	-0.045	-0.236	0
-1	3.129	3.179	0.0188	-0.037	-0.042	0
-0.8	2.415	2.471	0.0145	-0.0265	-0.179	0
-0.6	1.826	1.836	0.0043	-0.0165	-0.069	0
-0.4	1.342	1.377	-0.0004	-0.0071	-0.056	0.188
-0.2	1.212	1.221	-0.0092	0.0022	0.332	0
0	1.138	1.178	-0.0158	0.0035	1.352	0
0.2	1.202	1.287	-0.0109	0.0138	0.457	0
0.4	1.416	1.501	-0.0206	0.0182	0.463	0
0.6	1.76	1.892	-0.0357	0.0221	1.253	0
0.8	2.255	2.415	-0.0427	0.0264	1.071	0
1	2.871	3.115	-0.052	0.0341	0.632	0
1.2	3.673	3.874	-0.0571	0.0415	0.491	0
1.4	4.219	4.557	-0.0684	0.0567	0.495	0
1.6	4.907	5.207	-0.0675	0.057	0.382	0
1.8	5.441	5.673	-0.0852	0.063	0.379	0
2	6.281	6.655	-0.0883	0.0685	0.219	0

Table A6: Data for x- coma aberration.

Aberration coefficients	Beam Quality $(M^2)_x$	Beam Quality $(M^2)_y$	Divergence, θx	Divergence, θy	Waist location, Z_x	Waist location, Z_y
-2	12.24	6.764	0.1297	0.0469	-0.131	-0.06
-1.8	10.744	6.112	0.1263	0.0413	-0.152	-0.035
-1.6	9.454	5.147	0.1003	0.0321	-0.141	-0.122
-1.4	7.824	4.313	0.0837	0.0285	-0.097	-0.014
-1.2	6.664	3.624	0.0715	0.0185	-0.152	0
-1	5.639	2.949	0.0564	0.0167	-0.238	-0.029
-0.8	4.442	2.302	0.0457	0.0126	-0.338	-0.014
-0.6	3.153	1.749	0.0186	0.0032	-0.304	-0.067
-0.4	1.928	1.369	0.0122	0.001	-0.622	0.006
-0.2	1.231	1.192	-0.0011	-0.0017	-0.054	0.14
0	1.135	1.191	-0.0193	0.0029	1.538	0
0.2	1.446	1.301	-0.0292	-0.0005	0.362	0
0.4	1.848	1.438	-0.0373	-0.0059	0.985	0
0.6	3.089	1.812	-0.0466	-0.0106	0.514	0
0.8	4.34	2.252	-0.0586	-0.0159	0.29	0
1	5.805	2.953	-0.0856	-0.0235	0.223	0
1.2	7.238	3.708	-0.0774	-0.0268	0.123	0
1.4	8.715	4.553	-0.0936	-0.0283	0.086	0.086
1.6	10.378	5.555	-0.0901	-0.0308	0.068	0.043
1.8	11.455	6.302	-0.1093	-0.0333	0.088	0.006
2	12.72	7.274	-0.1173	-0.0299	0.042	0

Table A7: Data for y- coma aberration.

Aberration coefficients	Beam Quality $(M^2)_x$	Beam Quality $(M^2)_y$	Divergence, θx	Divergence, θy	Waist location, Z_x	Waist location, Z_y
-2	6.566	11.926	0.0685	0.2356	-0.215	-0.131
-1.8	5.846	10.944	0.0627	0.221	-0.222	-0.138
-1.6	4.993	9.122	0.044	0.1685	-0.319	-0.158
-1.4	4.176	8.064	0.0391	0.1675	-0.368	-0.171
-1.2	3.482	6.883	0.0336	0.1385	-0.476	-0.208
-1	2.783	5.726	0.0233	0.1194	-0.631	-0.275
-0.8	2.2	4.256	0.0126	0.0852	-0.545	-0.328
-0.6	1.727	3.235	0.0018	0.0691	-0.286	-0.192
-0.4	1.42	2.089	-0.0072	0.0481	0	0
-0.2	1.246	1.531	-0.0186	0.0237	0.679	0
0	1.139	1.19	-0.0176	0.0054	1.454	0
0.2	1.171	1.262	-0.0255	-0.0121	2.004	0.041
0.4	1.319	1.807	-0.0368	-0.0427	1.904	1.434
0.6	1.662	2.855	-0.043	-0.0574	1.35	0.883
0.8	1.937	3.874	-0.0463	-0.0791	1.413	0.635
1	2.59	5.234	-0.0552	-0.1164	0.894	0.434
1.2	3.387	6.966	-0.0669	-0.1277	0.64	0.248
1.4	4.003	8.12	-0.0704	-0.1337	0.523	0.178
1.6	4.757	9.363	-0.0764	-0.175	0.397	0.155
1.8	5.766	10.84	-0.0874	-0.2014	0.263	0.108
2	6.655	12.452	-0.0968	-0.2076	0.218	0.084

Table A8: Data for spherical aberration.

Aberration coefficients	Beam Quality $(M^2)_x$	Beam Quality $(M^2)_y$	Divergence, θx	Divergence, θy	Waist location, Z_x	Waist location, Z_y
-2	13.755	14.246	0.4785	0.5124	-0.187	-0.189
-1.8	12.756	13.092	0.4885	0.524	-0.225	-0.231
-1.6	11.559	12.166	0.4693	0.4983	-0.275	-0.274
-1.4	10.338	10.817	0.4475	0.4622	-0.326	-0.315
-1.2	8.675	8.989	0.4284	0.4543	-0.299	-0.283
-1	7.773	7.894	0.3893	0.4103	-0.08	-0.049
-0.8	5.695	5.896	0.3246	0.3529	-0.451	-0.482
-0.6	4.048	4.441	0.2529	0.2872	-0.72	-0.865
-0.4	2.628	2.577	0.1671	0.1962	-0.099	-0.878
-0.2	1.565	1.433	0.0713	0.0964	0	0
0	1.131	1.178	-0.0177	0.0046	1.292	0
0.2	1.558	1.7	-0.0968	-0.0847	0.042	0
0.4	2.543	2.85	-0.1946	-0.1822	0.914	0.701
0.6	4.092	4.724	-0.2807	-0.2847	0.807	0.745
0.8	5.456	6.13	-0.3272	-0.3314	0.495	0.386
1	6.998	8.013	-0.3625	-0.3787	0.071	0
1.2	8.416	9.081	-0.4016	-0.4034	0.037	0.024
1.4	9.523	10.397	-0.427	-0.4514	0.336	0.322
1.6	10.874	11.718	-0.4529	-0.4904	0.267	0.249
1.8	12.229	12.823	-0.4741	-0.5033	0.21	0.192
2	12.861	13.277	-0.4598	-0.476	0.169	0.169

Table A9: Data for x- tilt aberration.

Aberration coefficients	Beam Quality $(M^2)_x$	Beam Quality $(M^2)_y$	Divergence, θx	Divergence, θy	Waist location, Z_x	Waist location, Z_y
-2	1.938	1.488	-0.0351	0.0005	0.931	0
-1.8	1.798	1.41	-0.0252	-0.0035	0.703	0
-1.6	1.934	1.381	-0.0244	-0.0008	0	0
-1.4	1.51	1.3	-0.0202	0.0007	1.315	0.043
-1.2	1.474	1.243	-0.0171	0.001	1.363	0.036
-1	1.302	1.261	-0.0218	0.0048	1.329	0
-0.8	1.255	1.221	-0.0195	0.0014	1.655	0
-0.6	1.201	1.204	-0.0171	0.0021	1.045	0
-0.4	1.183	1.185	-0.0131	0.002	1.25	0.05
-0.2	1.221	1.216	-0.0218	0.0014	0.882	0
0	1.137	1.188	-0.0193	0.0041	1.366	0
0.2	1.327	1.234	-0.0147	-0.001	0.817	0
0.4	1.343	1.229	-0.0146	0.0013	1.054	0
0.6	1.217	1.21	-0.0147	0.0009	1.343	0.009
0.8	1.493	1.284	-0.0157	0.0029	1.254	0
1	1.489	1.29	-0.017	0.0009	1.094	-0.049
1.2	1.388	1.31	-0.024	0.0011	1.555	0
1.4	1.631	1.319	-0.0115	0.0001	0.786	0.076
1.6	1.738	1.359	-0.0106	0.0064	0.115	-0.117
1.8	2.082	1.455	-0.0155	0.0034	0.012	0
2	2.033	1.486	0.0008	0.0045	0.053	-0.07

Table A10: Data for y- tilt aberration.

Aberration coefficients	Beam Quality $(M^2)_x$	Beam Quality $(M^2)_y$	Divergence, θx	Divergence, θy	Waist location, Z_x	Waist location, Z_y
-2	1.267	1.552	-0.0023	0.012	0.313	0
-1.8	1.226	1.429	-0.0027	0.0054	0.269	0
-1.6	1.312	1.846	-0.0028	0.0102	0.241	0
-1.4	1.226	1.537	-0.0029	0.0077	0.013	0
-1.2	1.22	1.433	-0.004	0.0174	0	0
-1	1.206	1.384	-0.0049	0.0062	0.251	-0.093
-0.8	1.188	1.41	-0.0042	0.0125	0.202	0
-0.6	1.167	1.253	-0.0041	0.0053	0.283	-0.12
-0.4	1.189	1.346	-0.0054	0.0116	0.395	-0.037
-0.2	1.155	1.231	-0.0043	0.0079	0.319	0
0	1.123	1.131	-0.0022	0.0022	0.211	0
0.2	1.151	1.197	-0.0062	0.0021	0.431	0
0.4	1.157	1.218	-0.0073	0.0078	0.703	-0.03
0.6	1.159	1.196	-0.0073	-0.001	0.601	0.034
0.8	1.159	1.201	-0.006	0.0059	0.635	0
1	1.202	1.307	-0.0052	0.0019	0.425	0
1.2	1.195	1.265	-0.0047	0.0103	0.404	0
1.4	1.233	1.398	-0.004	0.0008	0.328	0.008
1.6	1.24	1.304	-0.0051	0.001	0.346	-0.002
1.8	1.265	1.538	-0.0057	-0.0081	0.376	0.076
2	1.385	1.794	-0.0046	-0.0046	0.44	0.274

APPENDIX B

Balancing of Astigmatism and Spherical Aberration with Defocus

In order to work out the plane of measurement of a beam, a correction factor is required for all aberrations other than defocus due to a shifting of the Gaussian plane. Defocus simply means to observe a beam in a plane other than the plane of focus, the focal plane which is a distance *z* from the aperture. The focal plane occurs at a distance equal to the radius of curvature of the field or in this case a lens focal length *f*.

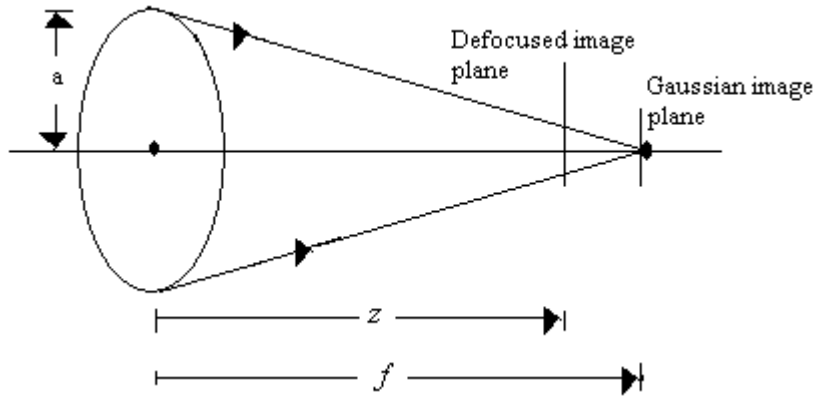

Fig B1: A beam focussed at a distance *f* but observed at a distance *z*.

At an arbitrary distance *z* from the focal plane, balanced defocus (B_d) is given by the seidel term (Mahajan, 1998):

$$B_d = \frac{1}{2}\left(\frac{1}{z} - \frac{1}{f}\right)a^2 \qquad \text{(B1)}$$

which has a value of zero when $z = f$ and is positive closer to the aperture and negative further from it. This means that the lens power *1/f*, is adjusted as:

$$\frac{1}{z} = \frac{1}{f} + \frac{2B_d}{a^2} \qquad \text{(B2)}$$

From Eqn. (B2), if the defocus coefficient can be worked out then the new focal length *z* of the lens can be determined correctly. The correction factors are:

- Spherical aberration, $\frac{1}{z} = \frac{1}{f} - \frac{12\sqrt{5}A_{40}}{a^2}$;
- Astigmatism, $\frac{1}{z} = \frac{1}{f} - \frac{2\sqrt{6}A_{22}}{a^2}$.

Substituting these conditions gives the Zernike balanced astigmatism and spherical aberrations.